

1 Title

2 SIGNIFICANCE OF PHYLLOSILICATE MINERALOGY  
3 AND MINERAL CHEMISTRY IN THE EPITHERMAL  
4 ENVIRONMENT. INSIGHTS FROM THE PALAI-ISLICA  
5 AU-CU DEPOSIT (ALMERÍA, SE SPAIN)

6

7 Authors

8 JAVIER CARRILLO-ROSÚA<sup>1</sup>; SALVADOR MORALES-RUANO<sup>2,3</sup>, IÑAKI ESTEBAN-  
9 ARISPE<sup>2</sup>, AND PURIFICACIÓN FENOLL HACH-ALÍ<sup>2,3</sup>

10

11 Address

12 <sup>1</sup> Departamento de Didáctica de las Ciencias Experimentales (Universidad de  
13 Granada), Facultad de Ciencias de la Educación, Campus de Cartuja, 18071,  
14 Granada, Spain

15 <sup>2</sup> Departamento de Mineralogía y Petrología (Universidad de Granada), Facultad de  
16 Ciencias, Avd. Fuentenueva s.n., 18002, Granada, Spain

17 <sup>3</sup> Instituto Andaluz de Ciencias de la Tierra (CSIC- Universidad de Granada),  
18 Facultad de Ciencias, Avd. Fuentenueva s.n., 18002, Granada, Spain.

19

20 Running title:

21 Significance of phyllosilicate mineralogy in the epithermal environment

22

23 Corresponding author:

24 JAVIER CARRILLO-ROSÚA

25 Departamento de Didáctica de las Ciencias Experimentales (University of Granada),  
26 Facultad de Ciencias de la Educación, Campus de Cartuja, 18071, Granada, Spain.

27 E-mail: [fjcarril@ugr.es](mailto:fjcarril@ugr.es)

28

**Abstract:**

29 X-ray diffraction, optical and electronic microscopy (scanning and  
30 transmitted), electron microprobe and Fourier transform infra red spectroscopy has  
31 been used to study phyllosilicates in the Palai-Islica Au-Cu epithermal, volcanic-  
32 hosted deposit, in order to link phyllosilicate mineralogy and mineral chemistry to  
33 ore genesis. Thus, different phyllosilicate assemblages characterize two types of  
34 mineralization, and related hydrothermal alteration. Chlorite and mica appear in  
35 polymetallic quartz veins with sulfides, and in the related chloritic and sericitic  
36 hydrothermal alteration. These minerals have notable textural and chemical  
37 differences (*i.e.* Fe/(Fe+Mg), Si and Al in chlorite and illitic and phengitic  
38 components in mica) amongst veins and altered rocks, revealing different genetic  
39 conditions. These chemical features also distinguish propylitic and regional, non ore-

40 related, low-temperature alteration. Hot hydrothermal fluids of near-neutral pH are  
41 responsible for vein mineralization and alteration. Illite, interstratified illite-smectite,  
42 kaolinite and pyrophyllite are characteristic, with a distribution pattern by zones, for  
43 the intermediate argillic and advanced argillic alteration around areas of  
44 silicification. In the latter, native gold appears associated to interstratified illite-  
45 smectite, suggesting a relatively low temperature formation. Hot, low-pH fluids are  
46 responsible for this mineralization and alteration assemblage. The present study  
47 contributes to epithermal models showing the co-existence of two different alteration  
48 styles in the same hydrothermal system.

49

50 **Keywords:**

51 Chlorite, epithermal, gold, mica, Spain, intermediate-sulfidation, volcanic-hosted

52

## INTRODUCTION

Hydrothermal ore deposits containing gold, silver and different base metals, have been extracted in the Cabo de Gata-Cartagena volcanic belt, in southeastern Spain, since 2000 BC. More than 3000 mining sites have been identified in the area and in the last century the region became one of the most important base-metal producers in Europe. In recent years the area has been the target of different mineral exploration companies looking for Au and Cu and mining activity has also taken place (*i.e.* Rodalquilar and Herrerias since 1992; Arribas *et al.*, 1995; Carrillo-Rosúa *et al.*, 2003c). These hydrothermal deposits range from epithermal to mesothermal, and vary enormously in their host rocks (rhyolites to andesites, schists or sedimentary rocks), ore mineral textures, associations, paragenetic sequences and proportions of precious metals (*e.g.* Morales-Ruano, 1994; Arribas and Tosdal, 1994; Arribas *et al.*, 1995; Morales-Ruano *et al.*, 2000). In the area there are also bentonitic-type clay deposits (formed at low temperature -  $< 100^{\circ}\text{C}$ , Leone *et al.*, 1983; Caballero *et al.*, 1985; Caballero *et al.*, 2005), extracted for industrial purposes.

Therefore a great variety of phyllosilicates and alteration assemblages could be expected in the Cabo de Gata-Cartagena volcanic belt, interesting for two reasons: firstly as an indicator of potential metalliferous deposits, and secondly as an industrial mineral in itself. Detailed mineralogical studies of phyllosilicates have been performed in the bentonitic low-temperature assemblage deposits (*e.g.* Caballero *et al.*, 2005 and references therein) whereas studies for the high-temperature group of deposits have been more partial/preliminary in nature (Arribas *et al.*, 1995; Morales-Ruano *et al.*, 2000).

Our research focuses on the Palai-Islica deposit, where recent exploration activity has demonstrated the presence of Au-Cu mineralization, related with the outcropping of an area of pervasive hydrothermal alteration (Morales-Ruano *et al.*, 2000). A study using X-ray diffraction (XRD), optical microscopy, scanning electron microscopy (SEM), electron microprobe (EPMA) and transmission electron microscopy (TEM), Fourier transform infra red spectroscopy (FTIR) was performed. The main object of this research is to characterize the mineralogy and mineral chemistry of phyllosilicates related with ore-mineralization, and to discuss hydrothermal alteration typology and its implication in ore genesis. This argument falls within the classification and discussion of epithermal deposits (*e.g.* Simmons *et al.*, 2005). This paper is noteworthy because it shows the co-existence of two different alteration styles in the same hydrothermal system. Special mention should also be made of the mineralogical transformation from volcanic rocks to phyllosilicates during hydrothermal activity, as well as the chemistry of phyllosilicates, and their relation to the conditions of the hydrothermal fluids.

## GEOLOGICAL BACKGROUND

The Palai-Islica is an Au-Cu epithermal deposit hosted by calc-alkaline rocks of the Cabo de Gata-Cartagena volcanic belt (Fig. 1a), which comprises part of the eastern

95 end of the Internal Zone of the Betic Cordillera. This neogene volcanic belt, with  
96 different series of volcanic rocks (*i.e.* calc-alkaline, shoshonitic, potassic calc-  
97 alkaline, ultrapotassic and basaltic series, López Ruiz and Rodríguez Badiola, 1980),  
98 formed within the context of compression, followed by an extensional event (Dewey,  
99 1988; García Dueñas *et al.*, 1992) and strike-slip movements in which volcanism  
100 occurs (*e.g.* Hernández *et al.*, 1987; Fernández Soler, 1996; Turner *et al.*, 1999).  
101 Associated with this magmatism, hydrothermal systems developed, being controlled  
102 by systems of faults and fractures. The hot fluids (up to 400-450°C, Morales Ruano,  
103 1994) reacted strongly with the host rocks and, in some districts mainly located  
104 inside calc-alkaline zone, gave rise to broad areas of alteration hosting metallic  
105 mineralization: Cabo de Gata (Pineda Velasco, 1984), Rodalquilar (*e.g.* Arribas *et*  
106 *al.*, 1995), and Palai-Islica (Morales-Ruano *et al.*, 2000; Carrillo-Rosúa *et al.*,  
107 2003a). The approximately 4 km<sup>2</sup> of Palai-Islica is one of these alteration areas (Fig.  
108 1b) which has become a recent target of mineral exploration companies for gold and  
109 copper (Morales-Ruano *et al.*, 2000). It appears near Carboneras town (Almería  
110 province, SE Spain) over an extensive zone of breccias and auto-breccias of  
111 andesites/dacites of ~10 Ma on age (Bellon *et al.*, 1983; Fernández Soler, 1996).  
112 These rocks (Fernández Soler, 1996), with a very porphyritic texture, are constituted  
113 by phenocrysts of bitownite plagioclase and hornblende (up to centimetre on size) ±  
114 clinopyroxene and orthopyroxene. In accessory amount there are quartz, Fe-Ti  
115 oxides, apatite and zircon.

116

117

#### SAMPLES AND METHODOLOGY

118 Samples were obtained from mineralization and from hydrothermally altered  
119 volcanic rocks at Palai-Islica. Two hundred and sixty-two samples selected from 21  
120 drill cores and surface sampling campaign had been studied. Whole-rock powders,  
121 oriented aggregates of <2µm fraction (with ethylene glycol and dimethyl sulfoxide  
122 solvation and without treatment), thin sections and a selection of ion milled  
123 specimens and suspension over Cu-grids of these samples, were prepared to  
124 determine the mineralogical, chemical and textural characteristics of phyllosilicates  
125 in this deposit. Transmitted light microscopy, XRD (Phillips PW 1710, with CuKα  
126 radiation, graphite monochromator and automatic divergence slit) at the Department  
127 of Mineralogy and Petrology of the University of Granada and SEM (Zeiss DSM  
128 950 and FESEM Leo Gemini 1530, with an EDX detector), EPMA (Cameca SX50,  
129 with WDX detector) and TEM (Philips CM20, with an EDAX solid-state EDX  
130 detector) at the “Centro de Instrumentación Científica” of the University of Granada  
131 had been used.

132

133

134

135

136

A total of 461 micro-analyses of phyllosilicate were obtained with different  
techniques (368 EPMA, 76 SEM and 18 TEM). Natural and synthetic-certified  
standards were used to calibrate EPMA, SEM and TEM-AEM quantitative analyses.  
The operating conditions were: 20 kV (EPMA and SEM), 200 kV (TEM)  
accelerating potential, 30nA (EPMA) and 1-2 nA (SEM) beam current, and

137 acquisition time of 40-100 s (for X-ray peak and background for EPMA), 100 s  
138 (SEM, TEM). Shorter counting times was used for K and Na in TEM-AEM analyses  
139 (30 s) and EPMA (20 s at peak and 20 s at background) to minimize alkali loss  
140 (Nieto *et al.*, 1996). AEM analysis were performed using a raster of 1000 x 200Å in  
141 scanning mode for ion-milled samples and a analytical window of 1µm x 1µm in  
142 scanning transmission mode for powders dispersed over holey C-coated formvar Cu  
143 grids. The acquired EPMA X-ray intensities were corrected for atomic number,  
144 mass-absorption and secondary fluorescence effects using the CAMECA-PAP  
145 version of the Pouchou and Pichoir (1984) procedure. The transformation of  
146 intensity ratios to concentration ratios in AEM analysis was made following the  
147 procedure of Cliff and Lorimer (1975). Structural formulas of chlorite and mica were  
148 calculated on the basis of O<sub>10</sub>(OH)<sub>2</sub> and 22 and 28 negative charges, O<sub>10</sub>(OH)<sub>8</sub> and  
149 O<sub>10</sub>(OH)<sub>2</sub> respectively.  
150 Four samples kaolinite (prepared as standard KBr pellets) were also analyzed by  
151 Nicolet 20SXB (“Centro de Instrumentación Científica” of the University of  
152 Granada) in order to obtain FTIR spectra and discriminate among kaolinite  
153 polytypes.

#### 154 PREVIOUS DATA ABOUT THE MINERALIZATION

155 Two different types of mineralization, quartz veins and veinlets with sulfides and  
156 dissemination in the silicification, are recognized in the Palai-Islica deposit (Fig. 2,  
157 Carrillo-Rosúa *et al.*, 2003a). Associated with this mineralization appears  
158 andesites/dacites which present an important hydrothermal alteration, although  
159 different in relation with both types of mineralization.

160  
161 (a) *Veins and veinlets of quartz with sulfides.* It is the main ore of the deposit,  
162 being located at depth between +70 and -90 meter above sea level (m.a.s.l.). These  
163 veins, sometimes stockwork-like and very penetrative, are very rich in sulfides.  
164 Although these veins have a sub-vertical trend, two main sub-horizontal levels have  
165 been recognized with enrichment in Au, Ag, Zn, Pb, Cd, As and Sb, with free gold  
166 grains and with fluid inclusions showing distinct characteristics (wide variation in  
167 salinity, 20 - 30 wt. % eq. NaCl, over a narrow temperature range - 200 to 250°C)  
168 relative to the rest of the deposit (Morales-Ruano *et al.*, 2000). Ore mineralogy  
169 consists in pyrite with occasionally high contents of chalcopyrite, sphalerite and  
170 galena. Accessory phases are very diverse, being Au-Ag alloys and different Ag-  
171 bearing sulfides and sulfosalts the most outstanding from an economic point of view  
172 (Carrillo-Rosúa *et al.*, 2002, 2003a and b, 2008a). The main gangue minerals are  
173 quartz, white mica (“sericite”), and chlorite with minor quantities of barite, gypsum,  
174 dolomite and siderite (Carrillo-Rosúa *et al.*, 2003a).

175 In relation to hydrothermal alteration, the andesites/dacites, which host the  
176 veins, are totally transformed to quartz, white mica plus chlorite, and, to a lesser  
177 extent, pyrite, dolomite, albite and epidote (Carrillo-Rosúa *et al.*, 2003a).  
178 Hydrothermal alteration is pervasive and the only minerals which remain alteration

179 are quartz, zircon and apatite, although the last suffers chemical transformation  
180 (Carrillo-Rosúa *et al.*, 2005). White mica and chlorite ( $\pm$ pyrite, albite and epidote) is  
181 the mineral assemblage in the proximal zones of the hydrothermal alteration. Only in  
182 distal zones, in the limit of the deposit, major phenocrysts could remain unaltered:  
183 first plagioclase, and in the less altered zones, hornblende and pyroxene. The  
184 alteration in the limit of the deposit could be defined as propylitic, with chlorite,  
185 epidote and calcite/dolomite.

186 (b) *Dissemination in the silicification*, which consists of complete  
187 replacement of the volcanic rock by quartz. Sometimes it is very porous, with holes  
188 corresponding with old volcanic phenocrysts, like *vuggy silica* textures. It is found at  
189 the surface of the deposit between +70 and +100 m.a.s.l. Ore minerals, mainly  
190 disseminated in holes, are very scarce being the mineralogy very flat: mainly pyrite  
191 with minor Cu-sulfides and native gold and copper (Carrillo-Rosúa *et al.*, 2002).  
192 Apart from the typical coarse-grained quartz, the gangue minerals comprise  
193 microcrystalline quartz, white mica (“sericite”) and barite, gypsum, jarosite,  
194 natrojarosite and natroalunite in latter veins.

195 The silicification has halos of advanced argillic and intermediate argillic  
196 alteration characterized by quartz, pyrophyllite, kaolinite, illite and interstratified  
197 illite-smectite. In distal zones, propylitic alteration also appears.

198

#### 199 MINERALOGICAL, TEXTURAL AND CHEMICAL CHARACTERISTICS OF 200 THE PHYLLOSILICATES

201 It is noteworthy the mineralogical differences, in especial in phyllosilicates, between  
202 both types of mineralization in the Palai-Islica deposit (Table 1). The main  
203 mineralogical, textural and chemical characteristics of the phyllosilicates in relation  
204 to described mineralization types and related hydrothermally altered host rock are  
205 described.

206

#### 207 *Quartz veins with sulfides and related hydrothermal alteration*

208 The petrographic observation and the study of X-ray diffractograms in the veins and  
209 related hydrothermal alteration have revealed that phyllosilicates are very abundant,  
210 but only chlorite and white mica have been recognized.

211 *Chlorite textures*. It appears as spherulitic aggregates ( $\sim$ 100  $\mu$ m) and rarely as  
212 inclusions in pyrite grains in the quartz veins (Fig. 3a). This spherulitic aggregates  
213 show lighter rims in respect to cores in backscattered images (Fig. 3b).

214 Chlorite also appears replacing amphibole, pyroxene and the groundmass in  
215 the hydrothermal alteration. Chlorite replacing mafic phenocrysts often develops  
216 bigger crystals than in replacing the groundmass and it is oriented. Thus, basal plane  
217 of chlorite is parallel to “b” and “c” axis of hornblende and pyroxene or, in other  
218 words, (001) plane of chlorite is parallel to (010) planes of amphibole and pyroxene  
219 (Fig. 3c and d). Occasionally, this mafic phenocrysts transformed to chlorite  
220 appears as “xenocrysts” inside the quartz veins (Fig. 3e). Chlorite very rarely

221 replaces plagioclase, being fine grained like generally in the groundmass and in  
222 some cases in mafic phenocrysts.

223 In the external zone characterized by propylitic alteration or even far from the  
224 deposit in zones of “regional” alteration due a widespread meteoric alteration,  
225 chlorite is also found replacing mafic phenocrysts, but generally fine grained  
226 disappearing orientated textures through outside of the veins (Fig. 3f). TEM studies  
227 of this chlorite show the existence of intercalations of 10 Å K-rich layers.

228  
229 *Chlorite mineral chemistry.* Table 2 and Figure 4 summarize chlorite  
230 microanalyses, being notably the chemical variability. Fe/(Fe+Mg) is directly  
231 proportional to Al<sub>total</sub> or <sup>IV</sup>Al and Mn and inversely proportional to Si (Fig. 4a, b and  
232 c). Si is inversely proportional to Al<sub>total</sub> (Fig. 4d). For the whole data, interlayer-  
233 cations (K+Na+2Ca) are proportional to octahedral vacancies although with higher  
234 slope for chlorite from the propylitic alteration than for chlorite from the  
235 hydrothermal alteration related to veins (Fig. 4e).

236 Chlorite from the different textural types has pronounced chemical  
237 differences in the Si, Al, Fe, Mg and Mn contents. Spherulitic aggregates of chlorite  
238 from the veins have the highest Al<sub>total</sub> (2.26 - 2.85 a.p.f.u.) and Fe/(Fe+Mg) ratio  
239 (0.56 – 0.78), low Si (2.65 – 3.05 a.p.f.u.), being variable the Mn content (0.02 –  
240 0.10 a.p.f.u.). Contrary to the whole analyses, not clear relations have been observed  
241 between different elements (Fig. 4a, b, c and d). Chemical zonation, due higher  
242 Fe/(Fe+Mg) ratio in the rimes that in the cores, is revealed by backscattered images  
243 (Fig. 3b). Chlorite in “xenocrysts” from the veins presents a chemical composition  
244 between chlorite in spherulitic aggregates in the veins and chlorite in the  
245 hydrothermal alteration.

246 Chlorite in the hydrothermal alteration related to veins has a high content of  
247 Si (2.89 - 3.14 a.p.f.u.), low in Al<sub>total</sub> (2.03 - 2.38 a.p.f.u.) and the lowest Fe/(Fe+Mg)  
248 ratio (0.05 – 0.40) of analyzed chlorites (Table 2). Chemical tendencies are the same  
249 than in the entirely analyses with the exception of Fe/(Fe+Mg) that is not related to  
250 Al<sub>total</sub> (Fig. 4a).

251 Chlorite in the propylitic hydrothermal alteration and regional alteration has a  
252 distinctive composition characterized by intermediate and homogeneous Fe/(Fe+Mg)  
253 ratio (0.30 – 0.43) and the highest Si (3.01 – 3.61 a.p.f.u.), interlayer-cations (0.01 –  
254 0.32 a.p.f.u.), and octahedral vacancies (0.09 – 0.87 a.p.f.u.). Chlorite from the  
255 properly propylitic alteration has intermediate Al (2.19 - 2.61 a.p.f.u.), high Mn (0.04  
256 – 0.06 a.p.f.u.) and K (average 0.08 a.p.f.u.), while chlorite in less altered rocks  
257 (propylitic to regional alteration) has low Mn (0.01 – 0.05 a.p.f.u.) and Al<sub>total</sub> (1.76 –  
258 2.28 a.p.f.u.), and high Ca (average 0.03 a.p.f.u.).

259 *White mica textures.* White mica is the most abundant phyllosilicate. It  
260 appears in the veins as crystals and aggregate of crystals of variable size, from sub-  
261 microscopic to a hundred of microns. Mica appears disseminated, intergrowth with

262 quartz, interstitial to quartz or even as inclusions in quartz, and also as micro-veins  
263 (Fig. 5a and b).

264 Mica is by far the most abundant phase replacing volcanic plagioclase (as  
265 phenocrysts or inclusions in amphibole and pyroxene). This mica varies from sub-  
266 microscopic to dozens of microns (typical “sericite”), occasionally with the (001)  
267 mica packet parallel to faces of the plagioclase (Fig. 5c and d) showing in TEM  
268 images a rare prismatic morphology (Fig. 5e). Mica also replaces maphic  
269 phenocrysts as sub-microscopic or microscopic disorientated crystals (Fig. 5f).  
270 Rarely mica aggregates also have a “palm” texture, but more frequent is coarse mica  
271 orientated in the maphic phenocrysts (Fig. 5g). In this last case, mica exclusively  
272 replaces the amphibole and pyroxene or it is accompanied by chlorite with the same  
273 orientation (Fig. 5h). In cases where mica and chlorite coexist, 10Å mica packets are  
274 found randomly interlayered in the chlorite stacks (Fig. 5i).

275 Mica also ranges from sub-microscopic to microscopic in the volcanic  
276 matrix, although fine grained crystals are much frequent.

277 The quartz veins are very penetrative. Thus, there is a wide range of  
278 transitional occurrences between proper veins and hydrothermally altered volcanic  
279 rock. For instance, in the veins it is frequent that mica presents characteristics of  
280 hydrothermal alteration: coarse grained that proceeds from the transformation of  
281 ferromagnesian phenocrysts and fine grained that precedes from the transformation  
282 of plagioclase (Fig. 5j).

283 Finally, although mica polytypism has not been systemically studied, *1M*,  
284 *2M* and *3T* polytypes has been deduced by XRD and TEM, the first mainly in the  
285 hydrothermal alteration and the third one only observed in the veins (Fig. 6a and b).

286 *White mica mineral chemistry.* Mica microanalyses have been summarized in  
287 Table 3, and Figure 7 and 8. The total interlayer-cations (K+Na+2Ca) range between  
288 0.65 and 0.82, being K the dominant cation, while total octahedral cations range  
289 between 1.99 and 2.15 a.p.f.u. The Fe/(Fe+Mg) ratio range between 0.08 and 0.82,  
290 although majority of data range between 0.08 and 0.43. Al<sub>total</sub> correlate inversely to  
291 Si (m~2, Fig. 7a), and interlayer-cations content does not correlate with Al<sub>total</sub> or Si  
292 (Fig. 7b and c). But there is a negative correlation between Fe+Mg and Al<sub>total</sub>, even  
293 better with <sup>VI</sup>Al (Fig. 7d), and a roughly positive correlation between Fe+Mg and Si  
294 (Fig. 7e). The Fe content is almost always lower than Mg content (Fe/(Fe+Mg)>0.5),  
295 presenting both elements a rough positive correlation (Fig. 7f).

296 The mica from different locations shows also some differences in its  
297 chemical composition. Mica in the veins has relatively high content of Al (2.20 –  
298 2.65 a.p.f.u.), K (0.60 – 0.82 a.p.f.u.) and F (0.00 – 0.08 a.p.f.u.), while Si content is  
299 low (3.23 – 3.44 a.p.f.u.) (Fig. 7 and 8). Fe+Mg is very variable reaching relatively  
300 high values (0.08 – 0.43 a.p.f.u.). The analyses with higher Fe+Mg, move away from  
301 the linear tendency of Fe+Mg *versus* Al<sub>total</sub> that show the majority of analyses (Fig.  
302 7d). Mica in the veins but originally precedent from the hydrothermal alteration  
303 shows a higher K and F content than mica directly originated in the veins (Fig. 8).

304 Mica in the hydrothermal alteration is characterized by a relatively high Si  
305 and low of K (0.60 – 0.77 a.p.f.u.) and total interlayer-cations (0.65 – 0.86 a.p.f.u.),  
306 and F (0.00 – 0.06 a.p.f.u.). It is also observed relatively coarse grained mica  
307 replacing plagioclase has lower Si and Fe and higher Al and K content than mica  
308 replacing ferromagnesian phenocrysts. In respect to fine mica which replaces  
309 plagioclase, that is relatively rich in Si, K, F and Fe and poor in Al in respect to the  
310 other types of mica in the hydrothermal alteration (Fig. 7 and 8, Table 3).

311

### 312 *Silicification and related hydrothermal alteration*

313 Phyllosilicates in the silicification are very scarce and correspond to interstratified  
314 illite-smectite. They appear as aggregates in micro-veins in which also appear native  
315 gold crystals (Fig. 9a). These micro-veins formed after the main quartz event  
316 generation, but before the formation of sulfates (barite → Fe-Al sulfates →  
317 gypsum). Very fine grained phyllosilicates (kaolinite, pyrophyllite, discrete illite and  
318 illite-smectite interstratified) + quartz are the most abundant phases in hydrothermal  
319 alteration that encloses silicification. It is possible to recognize a mineral zonation  
320 from the silicification to the most external zones of propylitic alteration (Fig. 2).

321 a) Proximal area: It is constituted by quartz, pyrophyllite, kaolinite, discrete  
322 illite and illite-smectite interstratified. Zones closer to the silicification are more  
323 quartz and pyrophyllite rich, the last mineral disappearing towards peripheral zones.  
324 It is observed that pyrophyllite have a major tendency to replace plagioclase, while  
325 quartz is enriched in the matrix. Kaolinite corresponds to kaolinite (± nacrite and  
326 dickte?) polytypes according to XRD and IR spectra patterns.

327 b) Distal zone: It is characterized by quartz, illite and interstratified illite-  
328 smectite.

329 The wide presence of interstratified illite-smectite it is deduced in X-ray  
330 diffractograms with ethylene-glycol solvation, being deduced a high proportion of  
331 illite layers (~ 90% according to Reynolds (1980)).

332 Electronic microscopy, mainly due TEM study, has confirmed interstratified  
333 illite-smectite is the only phyllosilicates found in the silicification. Backscattered  
334 images show changes in composition in several micron scale (Fig. 9b). In low  
335 magnification TEM images it is observed tabular phyllosilicates stacks up to several  
336 microns thick. Lattice-fringe images show layers always 10Å thick, and SAED  
337 patterns also show a 10Å periodicity, in a certain order pattern (Fig. 10). That is  
338 consistent with local ordered pattern in a major disorder sequence. A detailed  
339 observation of the lattice-fringe images show termination of several or individual  
340 layers in wedge (Fig. 10a and b). It is also observed splitting of 10Å layers in two 5Å  
341 layers that in hundred microns along distance fuse with its neighbour split layers  
342 (Fig. 10b). This structure could be related to screw dislocation, affecting to an  
343 interstratified illite-smectite.

344 *Phyllosilicate mineral chemistry.* Microanalysis in these phyllosilicates,  
345 except maybe TEM analyses (Tables 4 and 5), could correspond in a considerable

346 proportion to polycrystalline aggregates rather than individual crystal due the fine  
347 grain character of these phyllosilicates, being, therefore, very difficult interpret these  
348 analyses. These analyses reflect mixing between potassic illite with smectite, quartz,  
349 kaolinite and pyrophyllite as Figure 11 suggests.

350 The EPMA analyses of coarse phyllosilicates in the silicification (Table 4,  
351 Fig. 11) have low K (0.30 – 0.45 a.p.f.u.) and Al (1.57 - 2.27 a.p.f.u.) and high Si  
352 (3.65 – 4.21 a.p.f.u.), which suggests the presence of interlayered smectite. Change  
353 in backscattered image of these phyllosilicates is due a higher Si and lower Al  
354 content in the brighter zones than in the darker zones. That means there are domains,  
355 several microns in size, with higher proportions of smectite layers. AEM analyses of  
356 ion milled samples from the silicification have slight higher Al (2.29 – 2.40) and  
357 lower Si (3.45 – 3.55) being K similar (0.25 – 0.55 a.p.f.u.) than EPMA analyses.  
358 That is congruent with smectite layers are very penetrative, since micron size packets  
359 with illite composition have not been detected.

360 EPMA phyllosilicate analyses from distal alteration zone are very variable,  
361 although values up 0.79 and 2.42 a.p.f.u. of K and Al (similar to them of illite in  
362 relation to the veins and related alteration), has been found. Therefore, illite without  
363 smectite layers at micron size is presents in the distal alteration zone.

364  
365

## DISCUSSION

### *Characteristics of the transformation of volcanic rocks*

366 It has been deduced that substrate characteristics of host rock (chemistry and  
367 crystallography) have great importance in phyllosilicate mineralogy (Table 1) and  
368 texture in hydrothermal alteration in relation to veins. The volcanic matrix,  
369 constituted by glass or fine-grained crystals, develops chlorite and mica, and a large  
370 quantity of quartz. This non-crystalline (or fine-grained) protolith conditions both its  
371 high degree of reactivity (the volcanic matrix is the “easiest” microdomain to be  
372 altered by hydrothermal fluids) and the tendency to develop fine-grained phases. In  
373 contrast, mafic phenocrysts (hornblende and pyroxenes) mainly develop  
374 phyllosilicates (chlorite and mica). Chlorite is the main phyllosilicate which  
375 transforms mafic phenocrysts in conditions of relatively “weak” hydrothermal  
376 alteration: chloritic alteration and propylitic alteration (the weakest alteration type).  
377 This phenomenon is due to the fact that chlorite transformation implies a minor  
378 chemical change (amphibole and pyroxenes are Fe-Mg-Si-(Al)-bearing in the same  
379 way as chlorite). In many cases, chlorite is oriented in the mafic phenocrysts (Fig.  
380 3c, d). Thus, it is deduced the transformation is strongly conditioned by the crystal  
381 structure of the protolith (chain structure of Si tetrahedrons) which presents some  
382 crystallographic similitude with the layer Si tetrahedrons of chlorite. We propose,  
383 then, that hydrothermal fluids, firstly circulating through cleavage planes, produced  
384 amphibole/pyroxene dissolution: fluids were abundant, as is common in a  
385 hydrothermal system, and hot enough to enhance their reactivity. At the same time  
386 than mafic phenocrysts dissolution, epitaxial growth of (001) chlorite packets over  
387

388 (100) amphibole/pyroxene planes occurred (Fig. 12). Maybe, chlorite crystals with  
389 others orientations also nucleate. But these less abundant and smaller crystals, due  
390 the abundance of fluid could dissolve. The result is that crystal growth onto larger  
391 pre-existing oriented crystals is favoured, in a way similar to an Ostwald Ripening  
392 model (*e.g.* Eberl *et al.*, 1990) but accelerated for the high reactivity due the high  
393 fluid activity. Other types of transformation are rejected, such as the solid state  
394 transformation for illite-smectite proposed by Altner and Ylang (1997). The  
395 intervention of a large quantity of fluids could easily produce dissolution processes.

396 Only in propylitic alteration do we find relicts of hornblende, while further  
397 hydrothermal alteration produces total replacement of amphiboles/pyroxenes by  
398 chlorite.

399 Mica also replaces mafic phenocrysts, either as phyllosilicate alone, or  
400 intergrown with chlorite, mainly in zones of sericitic alteration. This mica or mica-  
401 chlorite intergrowth is also usually orientated with the (001) mica planes parallel to  
402 (100) amphibole/pyroxene planes. Our interpretation is that mica replaces chlorite,  
403 with an epitaxial mica growth over chlorite, and simultaneous chlorite dissolution.  
404 This occurs in a further hydrothermal alteration stage, with Mg-Fe loss and K  
405 incorporation in the rock. It is also possible mica and chlorite intergrowth, mainly in  
406 the chloritic-sericitic alteration zones, as suggest the presence of coherent mica –one  
407 layer- in chlorite stacks (Fig. 5i), maybe more difficult to explain with a dissolution  
408 (chlorite) -precipitation (mica) process.

409 Plagioclase phenocrysts are mainly replaced by mica, due to their lack of Fe  
410 and Mg, necessary for chlorite formation. This mica is finer-grained than the mica  
411 which replaces amphibole and pyroxene, reflecting a different crystallization  
412 process. Plagioclase tectosilicate structure does not normally condition a specific  
413 mica orientation, favouring nucleation rather than crystal growth. Only occasionally  
414 could (001) and (010) plagioclase cleavage planes constitute preferential places for  
415 growth of (001) packets of mica, sometimes with rare prismatic habit (Fig. 5d and e),  
416 these being the main channel of hydrothermal fluids during the alteration processes.  
417 The size of mica crystals in plagioclase, from sub-microscopic, to “sericite” size,  
418 could be related to the changes in the saturation state of hydrothermal fluids. Highly  
419 saturated fluids, usually linked only to sericitic alteration, could lead to sub-  
420 microscopic crystals formed in volcanic plagioclase (Fig. 5c), and sometimes also  
421 simultaneously formed in mafic phenocrysts.

422 In the hydrothermal alteration related to the silicification, the formation of  
423 phyllosilicates implies a lesser control of rock substrate than that seen in vein-related  
424 hydrothermal alteration. In this case, a lower pH in hydrothermal fluids enhances  
425 rapid dissolution processes, avoiding significant control of volcanic substrate  
426 chemistry in the crystallization of phyllosilicates, and also avoiding epitaxial  
427 phyllosilicate growth. Therefore, very fine, usually sub-microscopic phyllosilicate  
428 crystals (interstratified illite-smectite, illite, kaolinite and pyrophyllite), are formed  
429 indistinctly over the volcanic matrix, mafic phenocrysts and plagioclase.

430 Nevertheless as compared with phenocrysts, the matrix still favours quartz rather  
431 than phyllosilicate formation.

432

#### 433 *Implications of chlorite chemistry*

434 In the Palai-Islica, chlorites have a notable chemical variety linked to texture. Firstly,  
435 it is possible to distinguish between chlorites in the quartz veins and the related  
436 chloritic and sericitic alteration, and chlorites in the propylitic alteration. The main  
437 difference is the relatively homogeneous Fe/(Fe+Mg) ratio, and higher Si (Fig. 4d)  
438 content in the latter with respect to the former. Since chlorites are widespread in the  
439 region as a regional alteration feature, chemical analyses could be useful to detect  
440 signs of ore-bearing-related hydrothermal activity.

441 Secondly, the variable chemical composition of chlorite related to the  
442 hydrothermal fluids themselves is very notable: chlorite from the quartz veins;  
443 chlorite from the chloritic and sericitic alteration; and the differences between them.  
444 The Fe/(Fe+Mg) ratio is extraordinarily broad, between 0.05 and 0.78. This is one of  
445 the broadest found in a range of environments, such as metamorphic or  
446 diagenetic/very low grade metamorphic, but also geothermal fields and other  
447 hydrothermal deposits (Fig. 13). The observed Fe/(Fe+Mg) variation in  
448 hydrothermal Palai-Islica chlorite is related to the characteristics of the hydrothermal  
449 fluids and the mechanism of chlorite formation. Chlorite precipitated directly from  
450 the hydrothermal fluids, like chlorite aggregates in the veins, has a high Fe/(Fe+Mg)  
451 ratio, reflecting the chemical composition and perhaps also the temperature of the  
452 hydrothermal fluids (*e.g.* Kranidiotis and MacLean, 1987, Saccocia and Seyfried,  
453 1994). Nevertheless, chlorite produced by a transformation process (*i.e.* originating  
454 in the hydrothermal alteration) has a low Fe/(Fe+Mg) ratio, since its composition  
455 reflects the characteristics of hydrothermal fluids (*i.e.* composition and temperature)  
456 plus the composition of the substrate. Both mafic phenocrysts and the rock in  
457 general are relatively Mg rich, with low Fe/(Fe+Mg) ratio (Fig. 4). In addition,  
458 chlorites formed replacing phenocrysts, but subsequently incorporated within veins  
459 (Fig. 3d), have an intermediate composition. This signals that a higher interaction  
460 with the fluids increases the Fe/(Fe+Mg) ratio. In other words, hydrothermal fluids  
461 produce relatively high Fe chlorites by direct precipitation (also observable in other  
462 hydrothermal and geothermal environments, *e.g.* Kranidiotis and MacLean, 1987,  
463 Sanchez-España *et al.*, 2000; Hibti and Marignac, 2001; Zaccarini *et al.*, 2003;) and  
464 host rocks composition condition the reactant hydrothermal fluid chemistry in the  
465 host rock itself.

466 Si and Al, which correlate positively for ore-related hydrothermal chlorite (not  
467 in “propylitic” chlorite, Fig. 4d), are other components which clearly distinguish  
468 between chlorite from the quartz veins (higher in Al<sub>total</sub> and <sup>IV</sup>Al, and lower in Si  
469 content), and the hydrothermal alteration (lower in Al<sub>total</sub> and <sup>IV</sup>Al, and higher Si  
470 content). The correlation of Fe/(Fe+Mg) with Al (positive) and Si (negative) found

471 in the hydrothermal chlorite could be explained with Tschermack substitution  
472 ( $\text{SiMg} \leftrightarrow \text{IVAl}^{\text{VIAl}}$ ) (e.g. Walshe, 1986).

473 Octahedral vacancies are significant (0.04 – 0.29 a.p.f.u.) in chlorites from the  
474 veins and chloritic/sericitic alteration, and very abundant (0.09 – 0.87 a.p.f.u.) in  
475 chlorites from the propylitic alteration. Different studies have shown hydrothermal  
476 chlorite to have appreciable octahedral vacancies (e.g. McDowell and Elders, 1980:  
477 0.01 – 0.22; Cathelineau and Nieva, 1985: 0.02 – 0.42; Kranidiotis and MacLean:  
478 0.00 – 0.12; Fulignati *et al.*, 1997: 0.15 – 0.25 a.p.f.u.) in comparison with  
479 metamorphic chlorite, especially high-grade (Laird, 1988). Shau *et al.* (1990) and  
480 Jiang *et al.* (1994) associate these vacancies to the existence of mica or smectite  
481 layers or inclusions. In our study, this is the case for propylitic chlorite according to  
482 K+Na+2Ca contents (Fig. 4e) and TEM observations. But in chlorite from the  
483 veins and from chloritic/sericitic hydrothermal alteration, apparent vacancies are  
484 only partially related to a contamination effect of mica grains (Fig. 4e): they could  
485 also correspond with true vacancies, which existence have been demonstrate by  
486 Schmidt and Livi (1999).

487 Finally, Mn is a relatively abundant element in the chlorite studied (up to 0.10  
488 a.p.f.u.), more abundant than in chlorites from a sedimentary-metamorphic  
489 environment (e.g. Abad Martínez, 2002; Albee, 1962). It is even relatively high in  
490 comparison with other hydrothermal occurrences (e.g. Albee, 1962; Zaccarini *et al.*,  
491 2003). Mn in chlorite from Palai-Islica is roughly proportional to the Fe/(Fe+Mg)  
492 ratio (Fig. 4b), reaching higher values in chlorites from the veins. Therefore its  
493 concentration has much to do with ore-fluids. Association of Mn-bearing minerals  
494 with hydrothermal ore-bearing activity has been also highlighted in carbonate phases  
495 (Carrillo-Rosúa *et al.*, 2005).

496

#### 497 *Implications of mica chemistry*

498 Microprobe analyses of mica of different textural kinds show interlayer-charge  
499 between 0.65 a.p.f.u. and 0.86 a.p.f.u. Therefore a large number of analyses  
500 correspond to an illite-smectite composition (charge below 0.75 according to  
501 Newman and Brown (1987)). Nevertheless the numerous diffractograms never show  
502 modifications of (001) peaks after ethylene glycol solvation. The interlayer  
503 composition is dominantly potassic, while the paragonitic and margaritic component  
504 is very low (generally lower than 0.05 and 0.02 a.p.f.u. of Na and Ca respectively).  
505 In the octahedral layer, meanwhile, Fe+Mg (0.08 - 0.42 a.p.f.u.) content is  
506 considerably high, the octahedral charge usually being between 2 and 2.05. Fe  
507 content is almost always lower than Mg content, and usually very similar for each  
508 textural mica type, Mg content being the most variable (Fig. 7f). Therefore the  
509 Fe/(Fe+Mg) ratio is variable although in a lower range than in chlorite (mainly  
510 between 0.1 and 0.4).

511 Therefore, composition of this potassic octahedral mica could be explained by  
512 illitic ( $\text{Si}_{1-\square_1}\text{Al}^{\text{IV}}_{-1}\text{K}_{-1}$ ) and phengitic ( $(\text{Fe}+\text{Mg})_1\text{Si}_1^{\text{VI}}\text{Al}_{-1}^{\text{IV}}\text{Al}_{-1}$ ) substitution vectors.

513 The content of F in this mica is low, although significant (up to 0.08 a.p.f.u.). There  
514 are some differences between different textural mica types. Mica from the veins  
515 usually has a lower illitic component and more F than mica from the chloritic and  
516 sericitic alteration (Fig. 7a and 8d). The differences in the illitic component could be  
517 related to “disequilibrium” and even to formation temperature. It is known that  
518 muscovite “*sensu stricto*” began its formation in a very low-grade metamorphic  
519 environment, in epizone conditions, around 200°C (*e.g.* Abad Martínez, 2002). In the  
520 Palai-Islica mica system, however, no muscovitic composition has been found at  
521 temperatures as high as 300°C (Morales-Ruano *et al.*, 2000; Carrillo-Rosúa *et al.*,  
522 2003a). Similar non-muscovitic composition has been found in other Au epithermal  
523 deposits, such as Red Mountain (USA) or El Dorado (Chile). Even in these cases,  
524 more phengitic and illitic composition appears, but lower formation temperatures are  
525 also suggested (Bove *et al.*, 2002; Carrillo-Rosúa *et al.*, 2008b).

526 A complementary view could be deduced from the polytypism of Palai-Islica  
527 mica: the existence of different polytypes including *IM* polytype mainly in the  
528 hydrothermal alteration domain (Fig. 6), could suggest “variable disequilibrated  
529 conditions”.

530 Mica in the veins could be “less disequilibrated” than mica in the hydrothermal  
531 alteration on account of a higher fluid/rock ratio in the former as compared with the  
532 latter, rather than being due to the time factor, given that they could be formed  
533 during the same time interval. A higher temperature of mica from the veins could be  
534 another factor. Higher temperatures in other environments, such as very low-grade  
535 metamorphism, led to lower and more homogeneous illitic levels (*e.g.* Lee *et al.*,  
536 1986; López Munguira and Nieto, 2000; Abad Martínez, 2002). This aspect will be  
537 discussed in the specific geothermometry section below. Ore-forming fluids are  
538 clearly responsible for the introduction of F, as is also suggested by apatite chemistry  
539 (Carrillo Rosua *et al.*, 2005). Therefore F in mica could be used as a “chemical  
540 vector” related to the “intensity” of hydrothermal activity in a certain zone of the  
541 Palai-Islica deposit, and by extrapolation for other similar hydrothermal areas.

542 There are further chemical differences linked to specific mica textural groups.  
543 “Coarse” mica, replacing volcanic plagioclase, has a higher K and Al content, along  
544 with a lower Si, and a generally lower Fe content (this suggesting a higher illitic  
545 level), than mica which replaces amphibole and pyroxene. Microcrystalline mica,  
546 replacing volcanic plagioclase, has relatively high K, but also high Si and Mg, and  
547 low Al and Fe, suggesting a contamination of the analysis with some sub-  
548 microscopic chlorite. The cause for these chemical differences could be, again,  
549 related to kinetic problems and the types of crystallization processes. Mica that  
550 replaces plagioclase crystals is finer than mica replacing mafic phenocrysts, having  
551 a higher specific surface to equilibrate with the hot hydrothermal fluids, and is  
552 therefore less “disequilibrated”, *i.e.* less illitic in its composition. Moreover, in mica  
553 replacing amphiboles and pyroxenes, mica really replaces chlorite by chlorite

554 dissolution, epitactic mica crystallization favouring a Fe/(Fe+Mg) ratio similar to  
555 that of the chlorite which it replaces.

556 Finally, mica crystals in the veins which represent “xenocrysts” from the  
557 hydrothermal alteration have a relatively high F content compared with mica directly  
558 crystallized in the vein, reflecting a longer “history” of interaction with the F-bearing  
559 hydrothermal fluids.

560

#### 561 *Geothermometry*

562 Despite the questionable validity of chlorite thermometry (*e.g.* Shau *et al.*,  
563 1990; Jiang *et al.*, 1994), Walshe (1986), Kranidiotis and MacLean (1987) and  
564 Cathelineau (1988), equations have been tentatively applied and the results plotted in  
565 Figure 13. It is significant that the temperatures obtained by chlorite geothermometry  
566 for the veins are 75 – 150°C higher than in the hydrothermal alteration. Nevertheless,  
567 fluid inclusion data do not show higher temperatures of homogenization (Th) in the  
568 veins than in the hydrothermal alteration. In fact, they even show the opposite: the  
569 same mode value, but a higher range reaching lower Th (Carrillo-Rosúa, 2005). We  
570 could conclude the empirical chlorite geothermometers does not work at all in the  
571 case of Palai-Islica deposit. Or try to do further considerations if we consider it could  
572 works at least qualitatively (not quantitatively) within a certain system, as it could be  
573 the Palai-Islica deposit. Empirical observations (*e.g.* Kranidiotis and MacLean, 1987;  
574 Cathelineau, 1988) and thermodynamic calculations for high-variance assemblages  
575 (Vidal *et al.*, 2005) could support the second alternative.

576 We can do the following consideration. The measured fluid inclusions in the  
577 hydrothermal alteration are secondary in respect to the volcanic quartz phenocrysts,  
578 and are probably representative of “peak” conditions of the hydrothermal system. In  
579 this “peak” conditions fluids have enough energy to crack quartz phenocrysts and  
580 cause the fluid inclusions, while at lower temperatures hydrothermal fluids have not  
581 enough energy, and do not produce fluid inclusions. In the quartz veins, however,  
582 fluid inclusion better represents the full range of hydrothermal fluid activity since  
583 quartz is crystallizing and fluid inclusion are primary. Therefore it is possible that in  
584 the hydrothermal alteration the average temperature during the activity of the  
585 hydrothermal system could be lower than in the veins, although the peak (or peaks)  
586 would be the same. This would be in accordance with the chlorite geothermometry,  
587 but also with the illitic component of mica (related in some way with temperature,  
588 Cathelineau (1988)). Lower average temperature in the volcanic hydrothermally  
589 altered rocks than in the veins seems reasonable, and could be related to a drop in  
590 temperature of the hydrothermal fluids after leaving the main conduct channels  
591 (veins) and circulating through the host rocks (hydrothermal alteration). Alternative,  
592 could be related to a cooling of the fluids in the pores and cracks of the host rock in  
593 contact with neofomed minerals (and therefore with interaction mineral-fluid and  
594 possibility to modify mineral-chlorite...- composition) while the veins are sealed by  
595 mineralization processes.

596

597 *Alteration typology and genetic implications in ore deposition*

598 It is noteworthy that the two different gold-bearing mineralizations develop  
599 pervasive halos of hydrothermal alteration, but with significant mineral differences,  
600 especially in relation to phyllosilicate phases (Fig. 2).

601 The quartz veins with sulfides (the most important form of mineralization)  
602 are polymetallic (Cu, Zn, Pb, Au, Ag...) and sulphur-rich. Veins and their related  
603 hydrothermal alteration are characterised by dioctahedral mica and chlorite as  
604 phyllosilicate phases. This alteration could be defined as sericitic in zones where  
605 mica is the dominant mineral phase, and chloritic when chlorite is abundant (with  
606 possible presence of albite). The former represents a higher intensity of hydrothermal  
607 alteration. This means that the mineralization type and associated alteration are  
608 related to hydrothermal fluids, which are base and precious metal-bearing and of  
609 near-neutral pH. Furthermore, they have temperatures of 150–300°C according to  
610 fluid inclusion studies (Morales-Ruano *et al.*, 2000). These features coincide with an  
611 intermediate-sulfidation hydrothermal system (Hedenquist *et al.*, 2000).

612 The silicification is a type of mineralization which is poor in sulfide sulphur  
613 and base metals, although it contains high grades of gold. It develops a very different  
614 hydrothermal alteration. The core is constituted by the silicification containing ore  
615 gold-bearing mineralization. The silicification is surrounded by an advanced argillic  
616 envelope, mainly formed by pyrophyllite, kaolinite (with low disorder), illite and  
617 quartz. An outer-intermediate argillic envelope is constituted by illite and  
618 interstratified illite-smectite and quartz.

619 This silicification + advanced argillic alteration represents an intense leaching  
620 of the volcanic rock with lixiviation of the different cations present in the rock with  
621 the exception of Si + Al (argillic alteration), and only Si (silicification) in more  
622 extreme conditions. Very low pH fluids are deduced compatible with the formation  
623 of advanced argillic phyllosilicate assemblage (*e.g.* Reyes, 1990; Fialips *et al.*,  
624 1998), and are responsible for this extreme lixiviation process, coherent with a high-  
625 sulfidation hydrothermal environment (*e.g.* Hedenquist *et al.*, 2000). The transition  
626 of silicification to advanced argillic envelopes is explained by progressive fluid  
627 modification due to rock interaction in the movement of hydrothermal fluids from  
628 their feeder conduits, situated in silicification zones, to external areas. This  
629 progressive fluid modification would imply a rise in pH level and a fall in  
630 temperature, according to the mineralogical zonation: kaolinite located in outer  
631 zones, as compared with pyrophyllite, is of a lower temperature phase (*e.g.* Browne,  
632 1978; Henley and Ellis, 1983; Reyes, 1990). However, available fluid inclusion data  
633 (Carrillo-Rosúa, 2005) suggest the inexistence of appreciable changes in temperature  
634 of homogenization between silicification, advanced argillic alteration with  
635 pyrophyllite, and advanced argillic alteration with kaolinite. This Th, measured in  
636 secondary fluid inclusions in quartz volcanic phenocrysts, is mainly 260°C ± 30°C  
637 and seems to be too high for the presence of kaolinite, but appropriate to pyrophyllite

638 formation (Berman, 1988; Bjorkum and Walderhaugh, 1993). In hydrothermal  
639 systems it is assumed that kaolinite occurs at temperatures not higher than 200°C  
640 (e.g. Browne, 1978; Henley and Ellis, 1983; Reyes, 1990), while in diagenetic and/or  
641 very low-grade metamorphic sequences kaolinite transforms to become dickite at  
642 temperatures of 130°C (e.g. Ehrenberg *et al.*, 1993; Lázaro *et al.*, 2003). This  
643 apparent inconsistency between fluid inclusion and mineralogical data could be  
644 explained by kinetic effect. Hot hydrothermal fluids interact more (more fluids +  
645 more time) with the rock in the inner zone surrounding fluid conduits (*i.e.* the  
646 silicification and the inner zones of the advanced argillic envelope) than in outer  
647 zones of the advanced argillic envelope, where kaolinite appears.

648 The intermediate argillic alteration area characterized by illite and  
649 interstratified illite-smectite represents a less intense alteration and leaching area  
650 originated by higher pH fluids, in comparison to silicification and advanced argillic  
651 alteration zones. Its origin is related to the same hydrothermal fluids which produce  
652 silicification + advanced argillic envelope, although they are neutralized due to rock  
653 interaction and there may also be a lower fluid/rock ratio.

654 Seeing as its presence is not consistent with temperatures higher than 200°C  
655 (e.g. Merriman and Peacor, 1991), interstratified illite-smectite in the silicification  
656 and in the advanced argillic envelope could be related to a second stage in the  
657 formation of the silicification + argillic envelope. This second stage would be of  
658 lower temperature (<200°C) and higher pH in respect to the first stage, and, very  
659 significantly, is responsible for the gold mineralization. This is deduced from the  
660 association of native gold and direct precipitated interstratified illite-smectite  
661 aggregates (no illites without smectite interstratification have been found). This  
662 illite-smectite is very illite-rich, which could suggest a lower formation temperature,  
663 although still close to 200°C (e.g. Merriman and Peacor, 1991).

664 The interstratified illite-smectite in the intermediate argillic alteration zone  
665 could have been precipitated in the first hydrothermal stage due to a higher pH and  
666 lower temperature and fluid/rock ratio conditions in this more external area, but also  
667 in the second stage hydrothermal event.

668 Surrounding the chloritic and sericitic alteration zones (related to the quartz  
669 veins) as well as argillic and silicification areas, there is a zone of weak alteration  
670 that could be defined as propylitic. In this area, plagioclase phenocrysts could remain  
671 unaltered or with only some phyllosilicate crystals (*i.e.* illite and interstratified illite-  
672 smectite), while mafic phenocrysts are usually totally or partially altered to  
673 chlorite. The presence of epidote and calcite (rather than dolomite - which could  
674 appear occasionally in chloritic and sericitic alteration, Carrillo-Rosúa *et al.*, 2005) is  
675 also usually a characteristic feature.

676 Outside the Palai-Islica deposit, propylitic alteration becomes a regional  
677 alteration feature, with the disappearance of epidote. This propylitic alteration  
678 represents an area with a low infiltration rate of hydrothermal fluids, a low fluid/rock  
679 ratio, and the presence of other cool meteoric regional fluids. These are responsible

680 for the “regional alteration” and, mixed with a certain proportion of hydrothermal  
681 fluids, they originate propylitic alteration. Thus, these rocks have suffered a minor  
682 chemical change, reflected in the chlorite chemistry, with the Fe/(Fe+Mg) ratio equal  
683 to the mafic phenocrysts.

684

685

## CONCLUSIONS

686 Phyllosilicates are widespread phases among the mineralization and hydrothermal  
687 alteration zones in the Palai-Islica deposit. Two different phyllosilicate (alterations  
688 and/or neo-formed) assemblages have been distinguished in relation with two  
689 different kinds of ores: mica and chlorite associated with polymetallic gold and  
690 silver-rich veins; mica, interstratified illite-smectite, and kaolinite and pyrophyllite  
691 associated with gold dissemination in the silicification. The former, defined as  
692 chloritic and sericitic, is originated by near-neutral, highly metal-rich hydrothermal  
693 fluids, while the latter is produced by acidic, gold-bearing hydrothermal fluids in  
694 which a neutralization process and kinetic aspects determine a certain mineral  
695 zonation pattern (silicification → advanced argillic → intermediate argillic).  
696 Noteworthy here is that gold precipitation occurs at temperatures ≤ 200°C, which is  
697 lower than that responsible for the main hydrothermal alteration/silicification  
698 formation stage. This is due to its association with interstratified illite-smectite. A  
699 propylitic halo (chlorite, epidote, calcite-bearing) encloses the other alteration  
700 zones. Therefore, two epithermal environments have been identified in the same  
701 deposit: intermediate-sulfidation and high-sulfidation.

702 The advanced and intermediate argillic alteration zones develop very fine  
703 grain phyllosilicates, more concentrated in volcanic phenocrysts in respect to the  
704 matrix. This is related with a rapid, enhanced dissolution process due to the low pH  
705 of the hydrothermal fluids. In the chloritic and sericitic alteration zones, coarse-  
706 grained phyllosilicates (mainly inside mafic phenocrysts due to their anisotropic  
707 structure) and epitactic crystallization features (mafic phenocrysts → chlorite →  
708 mica) appear, suggesting a weaker dissolution process due to the near-neutral  
709 conditions of the hydrothermal fluids.

710 Chlorite and mica show a very wide compositional range. Chlorite chemistry,  
711 mainly Fe/(Fe+Mg) ratio, and Si and Al content, distinguishes between an origin  
712 related with high- or low- temperature fluids (*i.e.* chlorite of propylitic/regional  
713 alteration origin). In addition, these elements strongly differ in concentrations  
714 between chlorites in the hydrothermal alteration zone and that directly precipitated in  
715 the veins, thus suggesting different genetic conditions (*i.e.* fluid/rock ratio, influence  
716 of substrate, temperature...). Mica also presents some chemical composition  
717 differences according to its location: veins or hydrothermal alteration, the latter  
718 being richer in illitic component and poorer in F, directly related with ore-fluids. The  
719 composition and polytypism of mica suggest that equilibrium conditions have not  
720 been reached during hydrothermal activity.



- 763 Altaner, S.P. and Ylagan, R. (1997) Comparison of structural models of mixed-layer  
764 illite/smectite and reaction mechanisms of smectite illitization. *Clays and Clay*  
765 *Minerals*, **45**, 517-533.
- 766 Arribas, A. Jr. and Tosdal, R. (1994) Isotopic composition of Pb in ore-deposits of  
767 the Betic Cordillera, Spain. Origin and relationship to other European deposits.  
768 *Economic Geology*, **89**, 1074-1093
- 769 Arribas, A., Cunningham, C.G., Rytuba, J.J., Rye, R.O., Kelly, W.C., Podwysoki,  
770 M.H., McKee, E.H. and Tosdal, R.M. (1995) Geology, geochronology, fluid  
771 inclusions, and isotope geochemistry of the Rodalquilar gold alunite deposit,  
772 Spain. *Economic Geology*, **90**, 795-822.
- 773 Bailey, S.W. (1980) Structure of layer silicates. Pp. 1-123 in: *Crystal structures of*  
774 *clay minerals and their X-ray identification* (G.W. Brindley and G. Brown  
775 editors). Mineralogical Society, Monograph **5**, London.
- 776 Hibti, M. and Marignac, C. (2001) The Hajjar deposit of Guemessa (SW Mesta,  
777 Morocco): a metamorphosed syn-sedimentary massive sulphide ore body of the  
778 Iberian type of volcano-sedimentary massive sulphide deposits. Pp. 281-284 in:  
779 *Mineral deposits at the beginning of the 21st century* (A. Piestrzyński, *et al.*,  
780 editors). Balkema, Rotterdam, Netherlands.
- 781 Bellon, H., Bordet, P. and Montenat, C. (1983) Chronologie du magmatisme  
782 Néogène des Cordillères Bétiques (Espagne méridionale). *Bulletin de la*  
783 *Société Géologique de France*, **25**, 205-217.
- 784 Berman, R.G. (1988) Internally consistent thermodynamic data for stoichiometric  
785 minerals in the system Na<sub>2</sub>O- K<sub>2</sub>O-CaO-MgO-FeO- Fe<sub>2</sub>O<sub>3</sub>- Al<sub>2</sub>O<sub>3</sub>-SiO<sub>2</sub>-TiO<sub>2</sub>-  
786 H<sub>2</sub>O-CO<sub>2</sub>. *Journal of Petrology*, **29**, 445-522.
- 787 Bjorkum, P.A. and Walderhaugh, O. (1993) A model for the effect of illitization on  
788 porosity and quartz cementation sandstones. *Journal of Sedimentary Petrology*,  
789 **63**, 1089-1091.
- 790 Black, P.M. (1975) Mineralogy of New Caledonia metamorphic rocks: IV. Sheet  
791 silicates from the Ouegoa District. *Contribution to Mineralogy and Petrology*,  
792 **49**, 269-284.
- 793 Boles, J.R. and Franks, S.G. (1979) Clay diagenesis in Wilcox sandstones of  
794 southwest Texas: implications of smectite diagenesis on sandstones  
795 cementation. *Journal of Sedimentary Petrology*, **49**, 269-284.
- 796 Bove, D.J., Eberl, D.D., McCarty, D.K. and Meeker, G.P. (2002) Characterization  
797 and modelling of illite crystal particles and growth mechanism in a zoned  
798 hydrothermal deposit, Lake City, Colorado. *American Mineralogist*, **87**, 1546-  
799 1556.
- 800 Brimhall, G.H., Agee, C. and Stoffregen, R. (1985) The hydrothermal conversion of  
801 hornblende to biotite. *The Canadian Mineralogist*, **23**, 369-379.
- 802 Browne, P.R.L. (1978) Hydrothermal alteration in active geothermal fields. *Annual*  
803 *Review of Earth and Planetary Sciences*, **6**, 229-250.

- 804 Caballero, E., Reyes, E., Linares, J. and Huertas, F. (1985) Hydrothermal solutions  
805 related to bentonite genesis, Cabo de Gata Region, Almería, SE Spain.  
806 *Mineralogica et Petrographica Acta*, **29**, 187-196.
- 807 Caballero, E., de Cisneros, C.J., Huertas, F.J., Huertas, F., Pozzuoli, A. and Linares,  
808 J. (2005) Bentonites from Cabo de Gata, Almería Spain: A mineralogical and  
809 geochemical overview. *Clay Minerals*, **40**, 463-480.
- 810 Carrillo-Rosúa, F.J. (2005) *El depósito epitermal de oro-cobre Palai-Islica*  
811 *(Carboneras, Almería). Mineralogía, geoquímica y metalogenia*. PhD thesis,  
812 Univ. Granada., Spain.
- 813 Carrillo-Rosúa, F.J., Morales-Ruano, S. and Fenoll-Hach-Alí, P. (2002) The three  
814 generations of gold in the Palai-Islica epithermal deposit, Southeastern Spain.  
815 *The Canadian Mineralogist*, **40**, 1465-1481.
- 816 Carrillo-Rosúa, F.J., Morales-Ruano, S., Boyce, A.J. and Fallick, A.E. (2003a) High  
817 and intermediate sulphidation environment in the same hydrothermal deposit:  
818 the example of Au-Cu Palai-Islica deposit, Carboneras (Almería). Pp. 445-448  
819 in: *Mineral exploration and sustainable development* (D.G. Eliopoulos *et al.*,  
820 editors). Millpress, Rotterdam, Netherlands.
- 821 Carrillo-Rosúa, F.J., Morales Ruano, S. and Fenoll Hach-Alí, P. (2003b) Iron  
822 sulphides at the epithermal gold-copper deposit of Palai-Islica (Almería, SE of  
823 Spain). *Mineralogical Magazine*, **67**, 1059-1080.
- 824 Carrillo-Rosúa, F.J., Morales Ruano, S. and Fenoll Hach-Alí, P. (2008a) Textural  
825 and chemical features of sphalerite from the Palai-Islica deposit (SE Spain):  
826 implications for ore genesis and color. *Neues Jahrbuch für Mineralogie –*  
827 *Abhandlungen*, **185/1**, 49-64.
- 828 Carrillo-Rosúa, F.J., Morales Ruano, S., Fenoll Hach-Alí, P., Boyce, A.J., and  
829 Fallick, A.E. (2003c) Génesis de la barita de Las Herrerías y Sierra Almagrera.  
830 *Boletín de la Sociedad Española de Mineralogía*, **26-A**, 159-160.
- 831 Carrillo-Rosúa, F.J., Morales Ruano, S., Fenoll Hach-Alí, P., Morata Céspedes, D.,  
832 Belmar, M., Boyce, A.J. and Fallick, A.E. (2005) Mineralogical and chemical  
833 features of gangue phases in relation to hydrothermal mineralization and their  
834 host rocks. Pp. 1057-1060 in: *Mineral Deposit Research: Meeting the Global*  
835 *Challenge* (Y. Chen *et al.*, editors). Millpress, Rotterdam, Netherlands.
- 836 Carrillo-Rosúa, F.J., Morales-Ruano, S., Morata, D., Boyce, A.J., Fallick, A.E.  
837 Belmar, M. and Fenoll Hach-Alí, P. (2008b) Mineralogy and geochemistry of  
838 El Dorado epithermal gold deposit, El Sauce district, central-northern Chile.  
839 *Mineralogy and Petrology*, **92**, 341-360.
- 840 Cathelineau, M. (1988) Cation site occupancy in chlorites and illites a function of  
841 temperature. *Clay Minerals*, **23**, 471-485.
- 842 Cathelineau, M. and Nieva, D. (1985) A chlorite solid solution geothermometer. The  
843 Los Azufres (Mexico) geothermal system. *Contribution to Mineralogy and*  
844 *Petrology*, **91**, 235-244.

- 845 Cliff, G. and Lorimer, G.W. (1975) The quantitative analysis of thin specimens.  
846 *Journal of Microscopy*, **103**, 203-207.
- 847 Cooper, A.F. (1972) Progressive metamorphism of metabasic rocks from the Haast  
848 schist group of southern New Zealand. *Journal of Petrology*, **13**, 457-492.
- 849 Dewey, J.F. (1988) Extensional collapse of orogens. *Tectonics*, **7**, 1123-1140.
- 850 Eberl, D.D., Srdonon, J., Kralik, M., Taylor, B.E., Peterman, Z.E. (1990) Ostwald  
851 ripening of clays and metamorphic minerals. *Science*, **248**, 474-477.
- 852 Ehrenberg, S.N., Aagaard, P., Wilson, M.J., Fraser, A.R. and Duthie, M.L. (1993)  
853 Depth-dependent transformation of kaolinite to dickite in sandstones of the  
854 Norwegian continental shelf. *Clay Minerals*, **28**, 325-352.
- 855 Fernández Soler, J.M. (1996) *El vulcanismo calc-alcálico en el Parque Natural de*  
856 *Cabo de Gata-Níjar (Almería). Estudio volcanológico y petrológico*. PhD  
857 thesis, Univ. Granada, Sociedad Almeriense Historia Natural, Spain.
- 858 Fialips, C.I., Petit, S., Decarreau, A. and Beaufort, D. (1998) Effects of temperature  
859 and pH on the kaolinite crystallinity. *Mineralogical Magazine*, **62A**, 452-454.
- 860 Fulignati, P., Malfitano, G. and Sbrana, A. (1997) The Pantelleria caldera geothermal  
861 system: Data from the hydrothermal minerals. *Journal of Volcanology and*  
862 *Geothermal Research*, **75**, 251-270.
- 863 García Dueñas, V., Balanya, J.C. and Martínez Martínez, J.M. (1992) Miocene  
864 extensional detachments in the outcropping basements of the northern Alboran  
865 Basin (Betics). *Geomarine Letters*, **12**, 88-95.
- 866 Hecht, L., Thuro, K., Plinninger, R. and Cuney, M. (1999) Mineralogical and  
867 geochemical of hydrothermal alteration and episyenitization in the Königshain  
868 granites, northern Bohemian Massif, Germany. *Geologische Rundschau*, **88**,  
869 236-252.
- 870 Hedenquist, J.W., Arribas, M.A. and Gonzalez-Urrien, E. (2000) Exploration for  
871 epithermal gold deposits. Pp. 245 – 277 in: *Gold in 2000* (S.G. Hagemann and  
872 P.E. Brown editors). *Reviews in Economic Geology*, **13**.
- 873 Henley, R.W. and Ellis, A.J. (1983) Geothermal systems, ancient and modern. *Earth*  
874 *Science Reviews*, **19**, 1-50.
- 875 Hernández, J., de Larouzière, F.D., Bolze, J. and Bordet, P. (1987) Le magmatisme  
876 néogène bético-rifain et couloir de décrochement trans-Alboran. *Bulletin de la*  
877 *Société Géologique de France*, **3**, 257-256.
- 878 Hibti, M. and Marignac, C. (2001) The Hajjar deposit of Guemessa (SW Mesta,  
879 Morocco): a metamorphosed syn-sedimentary massive sulphide ore body of the  
880 Iberian type of volcano-sedimentary massive sulphide deposits. Pp. 281-284 in:  
881 *Mineral deposits at the beginning of the 21st century* (A. Piestrzyński, et al.,  
882 editors). Balkema, Rotterdam, Netherlands.
- 883 Instituto Geológico y Minero de España (1974) *Mapa Geológico de España*. Escala  
884 1:50,000. Hoja 1046 (24-42): Sorbas. Servicio de publicaciones Ministerio de  
885 Industria.

- 886 Jiang, W.T., Peacor, D.R. and Buseck, P.R. (1994) Chlorite geothermometry?-  
887 Contamination and apparent octahedral vacancies. *Clays and Clay Minerals*,  
888 **42**, 593-605.
- 889 Kranidiotis, P. and MacLean, W.H. (1987) Systematics of chlorite alteration at the  
890 Phelps Dodge massive sulphide deposit, Matagami, Quebec. *Economic*  
891 *Geology*, **82**, 1898-1911.
- 892 Laird, J. (1988) Chlorites: metamorphic petrology. Pp. 405-447 in: *Hydrous*  
893 *phyllosilicates /Exclusive of Micas* (S.W. Bailey editor). Review in  
894 *Mineralogy*, **19**, Mineralogical Society of America, Washington, D.C., USA.
- 895 Lázaro, C., Ruiz Cruz, M.D. and Sanz de Galdeano, C. (2003) Características  
896 metamórficas del Triásico Maláguide en las unidades intermedias del sector de  
897 Diezma (Sierra Arana, Cordillera Bética). *Boletín de la Sociedad Española de*  
898 *Mineralogía*, **26**, 123-136.
- 899 Lee, J.H., Peacor, D.R., Lewis, D.D. and Wintsch, R.P. (1986) Evidence for  
900 syntectonic crystallization for the mudstone to slate transition at Lehigh Gap,  
901 Pennsylvania, USA. *Journal of Structural Geology*, **8**, 767-780.
- 902 Leone, G., Reyes, E., Cortecchi, G., Pochini, A. and Linares, J. (1983) Genesis of  
903 bentonites from Cabo de Gata, Almería, Spain: A stable isotope study. *Clay*  
904 *Minerals*, **18**, 227-238.
- 905 López Munguira, A. and Nieto, F. (2000) Transmission electron microscopy study of  
906 very low-grade metamorphic rocks in Cambrian sandstones and shales, Ossa-  
907 Morena Zone, southwest Spain. *Clays and Clay Minerals*, **48**, 213-223.
- 908 López Ruiz, J. and Rodríguez Badiola, E. (1980) La región volcánica del sureste de  
909 España. *Estudios Geológicos*, **36**, 5-63.
- 910 Maxwell, D.T. and Hower, J. (1967) High grade diagenesis and low-grade  
911 metamorphism of illite in the Precambrian belt series. *American Mineralogist*,  
912 **52**, 843-857.
- 913 McDowell, S.D. and Elders, W.A. (1980) Authigenic layer silicate minerals in  
914 borehole Elmore 1, Salton Sea geothermal field, California, USA. *Contribution*  
915 *to Mineralogy and Petrology*, **74**, 293-310.
- 916 Merriman, R.J. and Peacor, D.R. (1991) Very low-grade metapelites: mineralogy,  
917 microfabrics and measuring reaction progress. Pp. 10-60 in: *Low grade*  
918 *metamorphism* (M. Frey and D. Robinson editors). Blackwell Science.
- 919 Moore, D.M. and Reynolds, R.C.Jr. (1997) *X-ray diffraction and the identification*  
920 *and analysis of clay minerals*. Oxford University Press, Oxford, 2<sup>nd</sup> edition.
- 921 Morales-Ruano, S. (1994). *Mineralogía, geoquímica y metalogenia de los*  
922 *yacimientos hidrotermales del SE de España*. PhD thesis, Univ. Granada,  
923 Spain.
- 924 Morales-Ruano, S., Carrillo-Rosúa, F.J., Fenoll Hach-Alí, P., de la Fuente Chacón,  
925 F. and Contreras López, E. (2000) Epithermal Cu-Au mineralisation in the  
926 Palai-Islica deposit, Almería, Southeastern Spain, fluid inclusion evidence of

- 927 mixing of fluids as guide to gold mineralisation. *The Canadian Mineralogist*,  
 928 **38**, 553-566.
- 929 Nieto, F., Ortega-Huertas, M., Peacor, D.R. and Aróstegui, J. (1996) Evolution of  
 930 illite/smectite from early diagenesis through incipient metamorphism in  
 931 sediments of the Basque-Cantabrian Basin. *Clays and Clay Minerals*, **44**, 304-  
 932 323.
- 933 Newman, A.C.D. and Brown, G. (1987) The chemical constitutions of clays. Pp. 1-  
 934 128 in: *Chemistry of Clays and Clay Minerals* (A.C.D. Newman editor).  
 935 Mineralogical Society, Monograph **6**, London.
- 936 Pouchou, J.L and Pichoir, F. (1984) Un nouveau modèle de calcul pour la  
 937 microanalyse quantitative per spectrométrie de rayons X. *La Recherche*  
 938 *Aéropatiale*, **3**, 167-192.
- 939 Pineda Velasco, A. (1984) Las mineralizaciones metálicas y su contexto geológico  
 940 en el área volcánica Neógena del Cabo de Gata (Almería, SE de España).  
 941 *Boletín Geológico Minero*, **95**, 569-592.
- 942 Reyes, A.G. (1990) Petrology of Philippine geothermal systems and the application  
 943 of alteration mineralogy to their assessment. *Journal of Volcanology and*  
 944 *Geothermal Research*, **43**, 273-309.
- 945 Reynolds, R.C. Jr. (1980) Interstratified clay minerals. Pp. 249-303 in: *Crystal*  
 946 *structures of clay minerals and their X-ray identification* (G.W. Brindley and  
 947 G. Brown editors). Mineralogical Society, Monograph **5**, London..
- 948 Saccocia, P.J. and Gillis, K.M. (1995) Hydrothermal upflow zones in the oceanic  
 949 crust. *Earth and Planetary Science Letters*, **136**, 1-16.
- 950 Saccocia, P.J. and Seyfried, W.E. (1994) The solubility of chlorite solid solutions in  
 951 3.2 wt % NaCl fluids from 300 - 400°C, 500 bars. *Geochimica et*  
 952 *Cosmochimica Acta*, **58**, 567-585.
- 953 Sánchez España, J., Velasco, F. and Yusta, I. (2000) Hydrothermal alteration of  
 954 felsic volcanic rocks associated with massive sulphide deposition in the  
 955 northern Iberian Pyrite Belt (SW Spain). *Applied Geochemistry*, **15**, 1265-  
 956 1290.
- 957 Schmidt, D. and Livi, K.J.T. (1999) HRTEM and SAED investigations of  
 958 polytypism, stacking disorder, crystal growth, and vacancies in chlorites from  
 959 subgreenschist facies outcrops. *American Mineralogist*, **84**, 160-170.
- 960 Shau, Y.H., Peacor, D.R. and Essene, E.J. (1990) Corrensite and mixed-layer  
 961 chlorite/corrensite in metabasalts from northern Taiwan: TEM/AEM, EMPA,  
 962 XRD, and optical studies. *Contribution to Mineralogy and Petrology*, **105**,  
 963 123-142.
- 964 Simmons, S.F., White, N.C. and John, D. (2005) Geological characteristics of  
 965 epithermal precious and base metal deposits. Pp 485-522 in: *Economic*  
 966 *Geology 100th Anniversary Volume 1905-2005*, (J.W. Hedenquist *et al.*,  
 967 editors). Society of Economic Geologist Inc., Littleton, Colorado, USA.

- 968 Turner, S.P., Platt, J.P., George, R.M.M., Kelley, S.P., Pearson, D.G. and Nowell,  
969 G.M. (1999) Magmatism associated with orogenic collapse of the Betic-  
970 Alboran domain, SE Spain. *Journal of Petrology*, **40**, 1011-1036.
- 971 Vidal, O., Parra, T., and Vieillard, P. (2005) Thermodynamic properties of the  
972 Tschermak solid solution in Fe-chlorite: Application to natural examples and  
973 possible role of oxidation. *American Mineralogist*, **90**, 347-358.
- 974 Walshe, J.L. (1986) A six-component chlorite solid solution model and the  
975 conditions of chlorite formation in hydrothermal and geothermal systems.  
976 *Economic Geology*, **81**, 681-703.
- 977 Zaccarini, F., Garuti, G., Rossi, A., Carrillo Rosúa, F.J., Morales Ruano, S. and  
978 Fenoll Hach-Alí, P. (2003) Application of chlorite and fluid-inclusion  
979 geothermometry to vein and stratiform Fe-Cu-Zn sulphide deposits of the  
980 northern appennine ophiolites (Emilia Romagna and Liguria, Italy). *Atti*  
981 *Ticinensi di Scienze della Terra*, **9**, 109-111.
- 982

# Figure 1. Carrillo et al

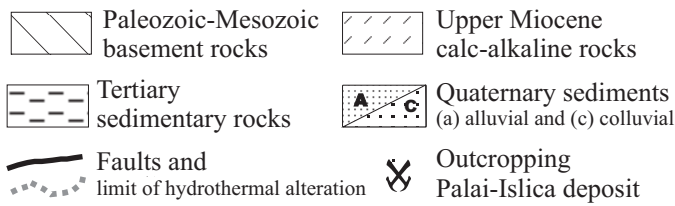
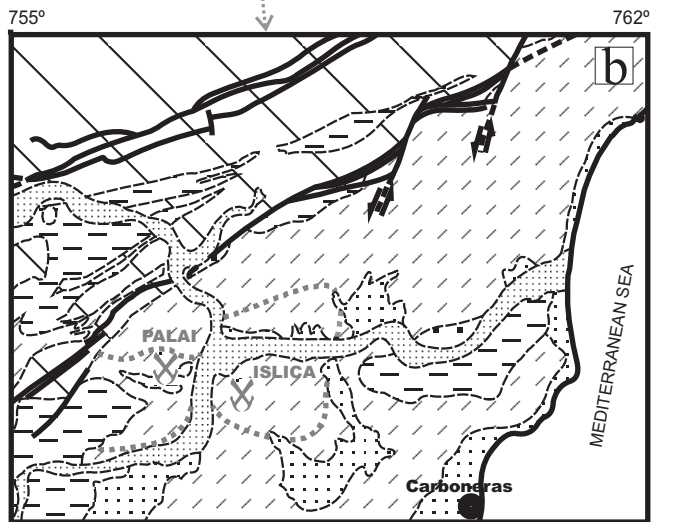
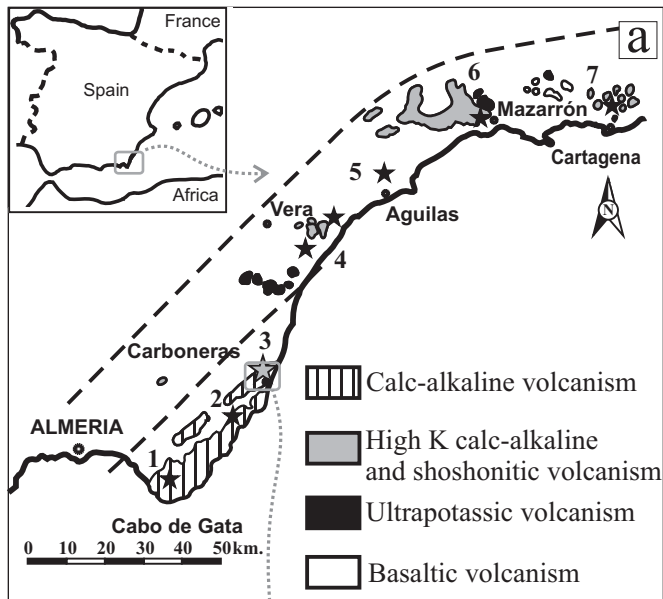


# Figure 2. Carrillo et al

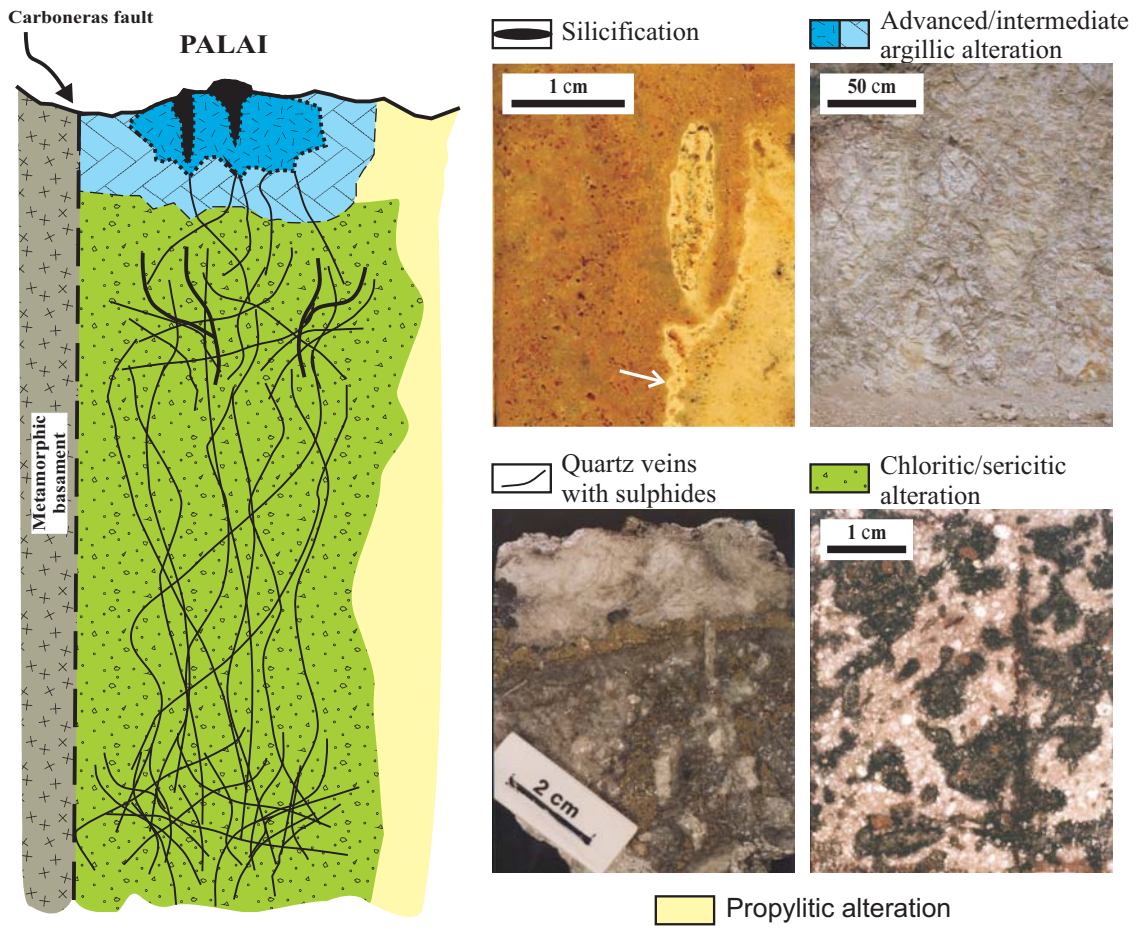
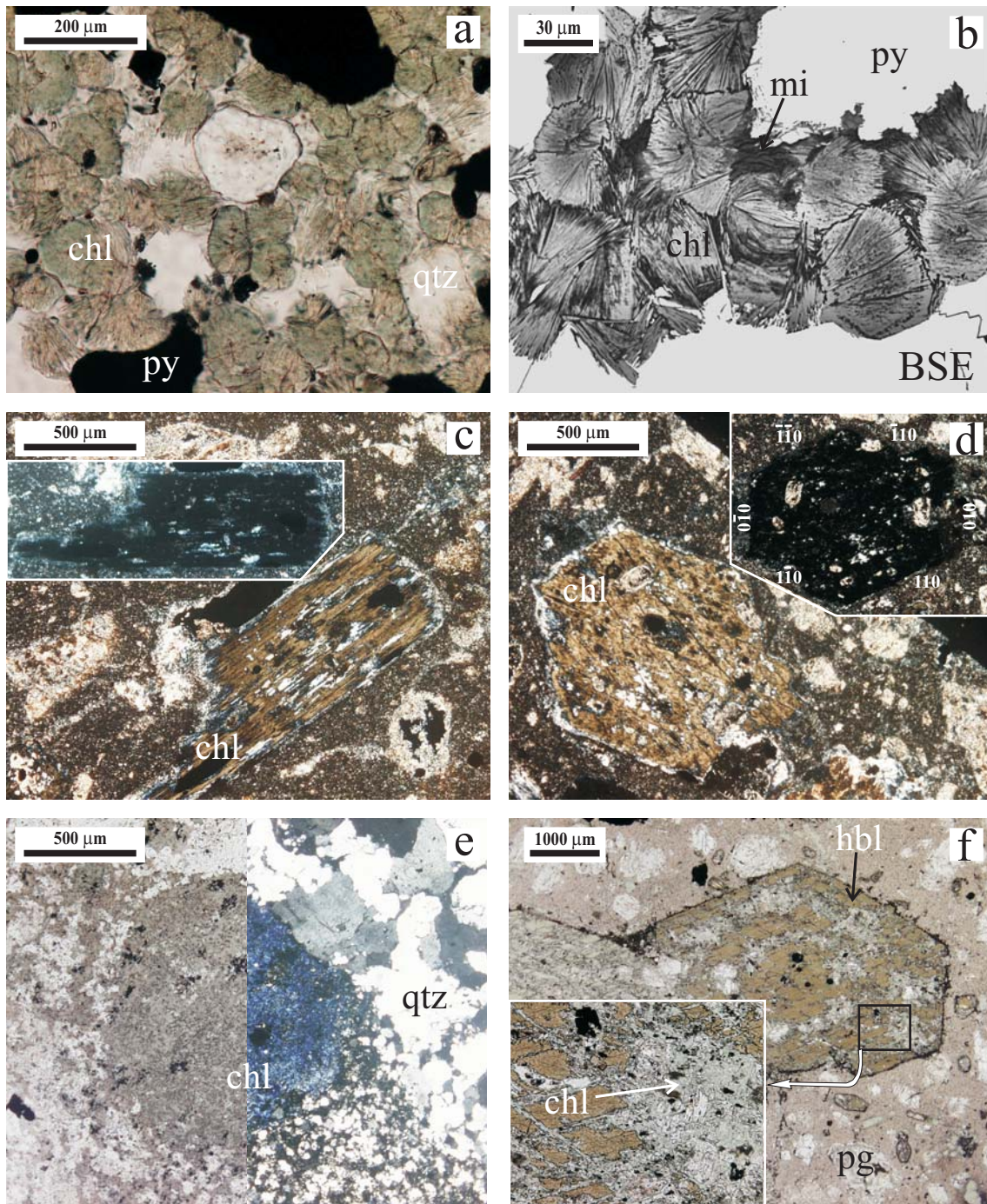


Figure 3. Carrillo et al



# Figure 4. Carrillo et al

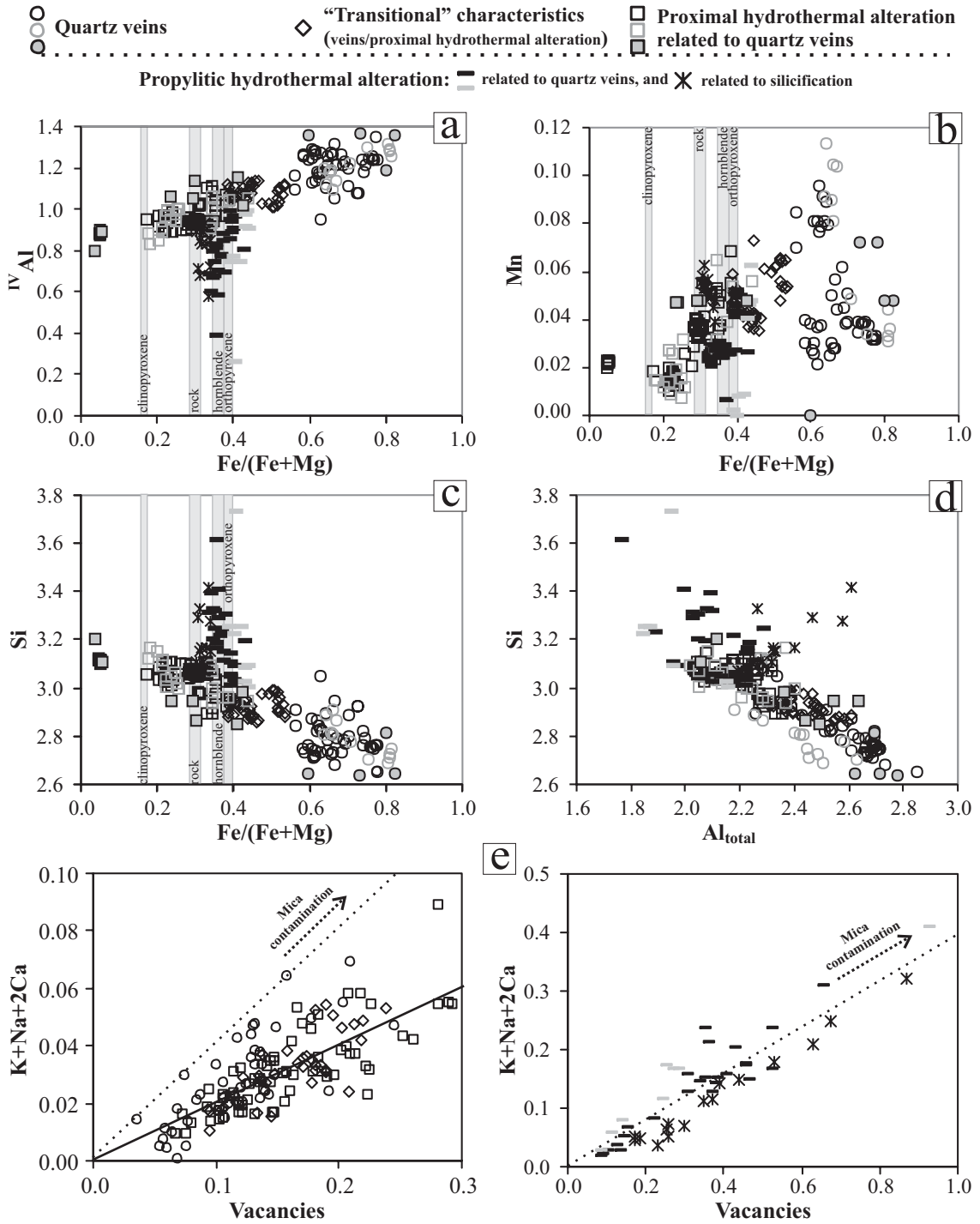
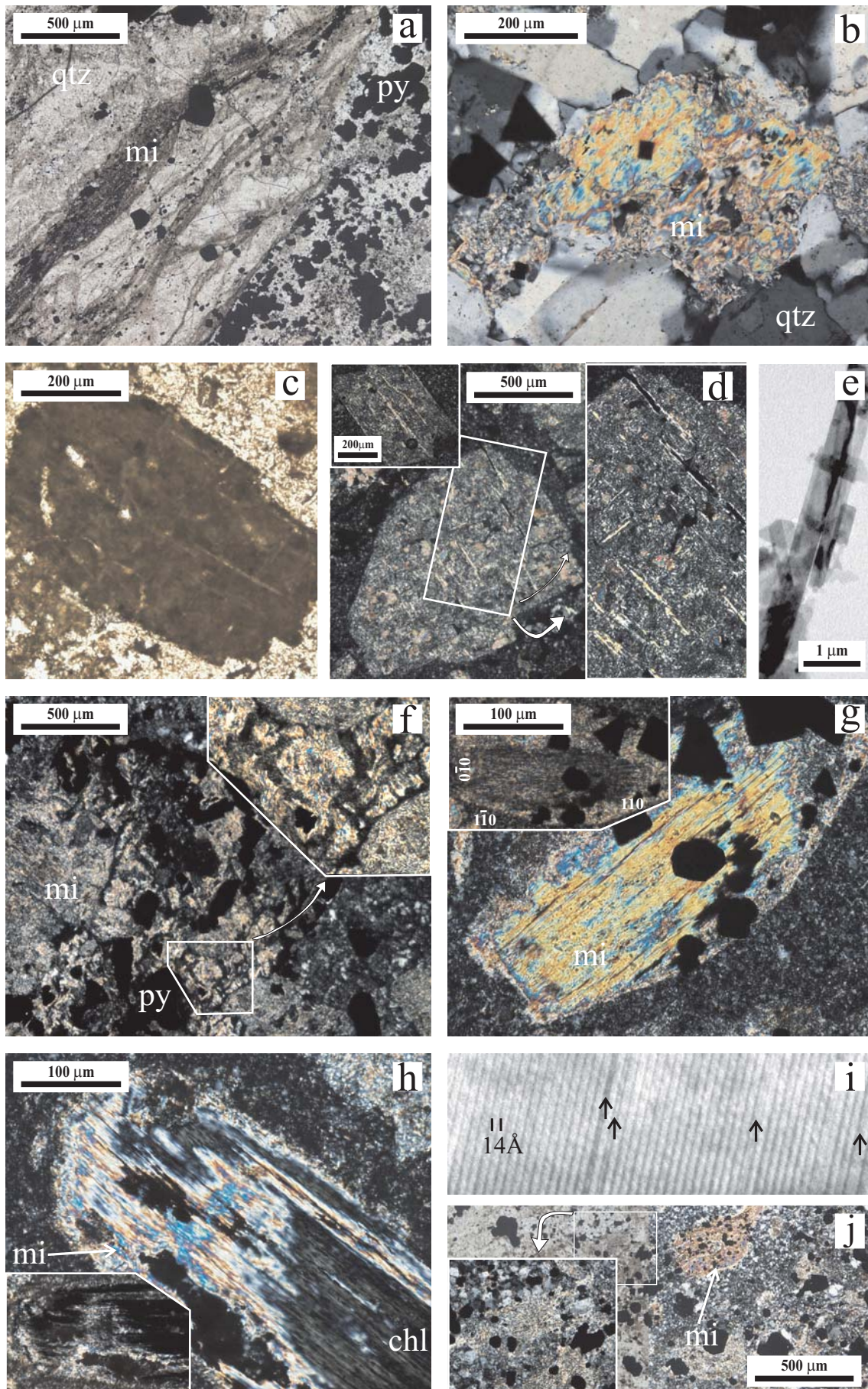
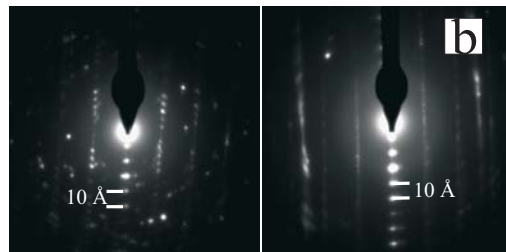
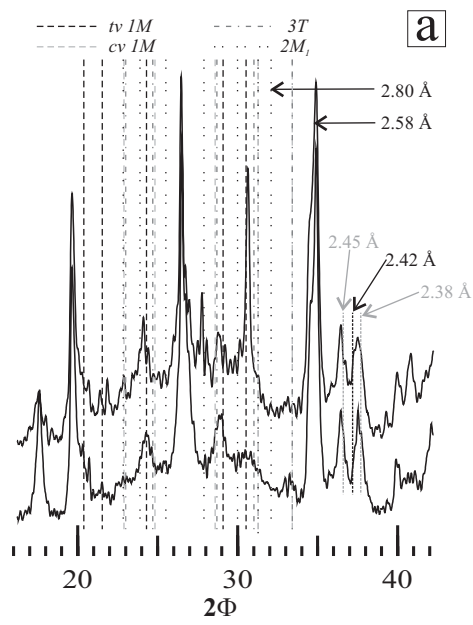


Figure 5. Carrillo et al



# Figure 6. Carrillo et al



# Figure 7. Carrillo et al

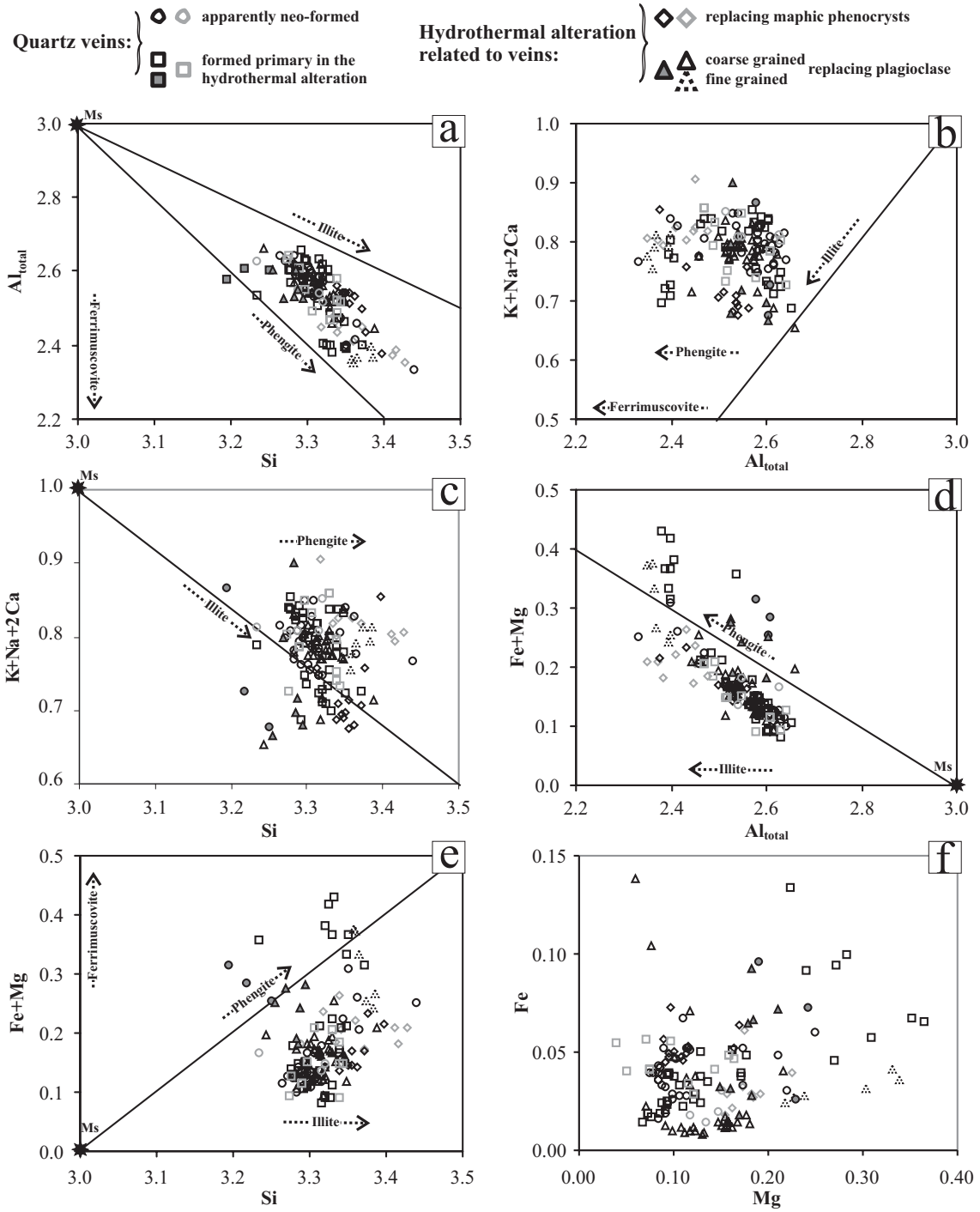


# Figure 8. Carrillo et al

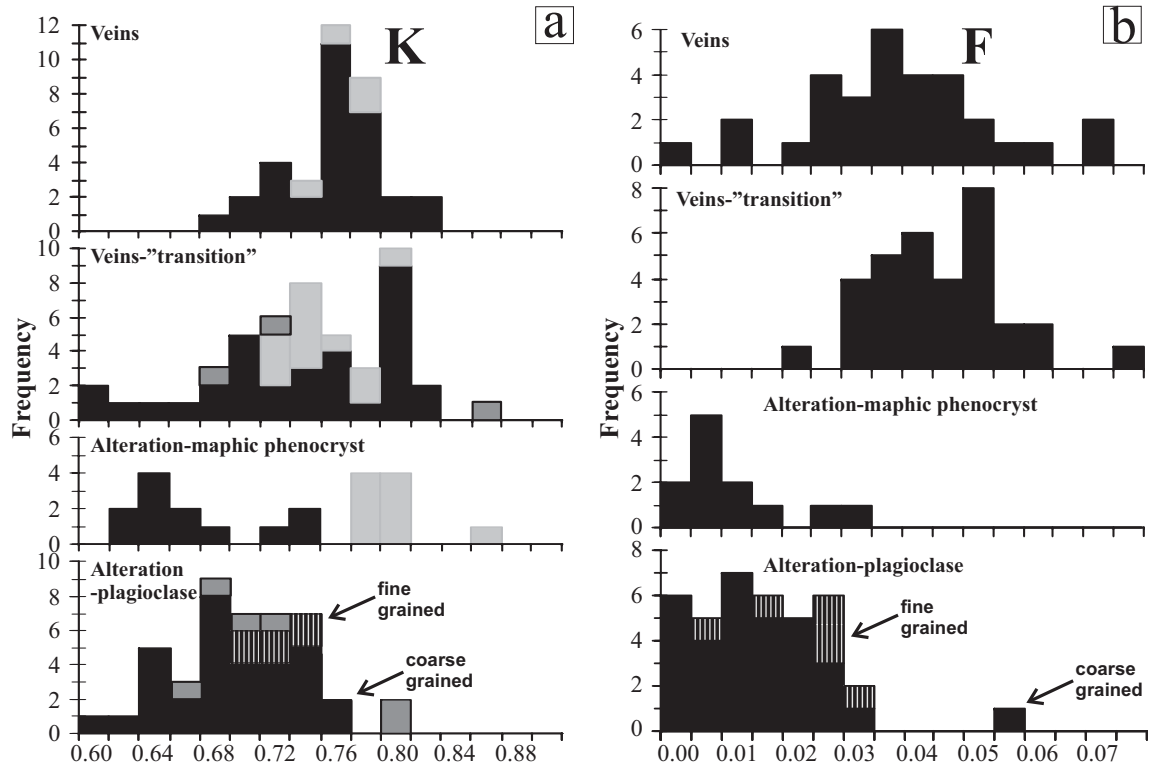


Figure 9. Carrillo et al

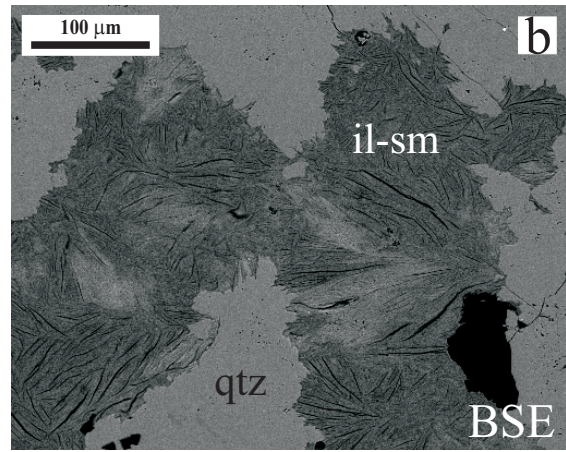
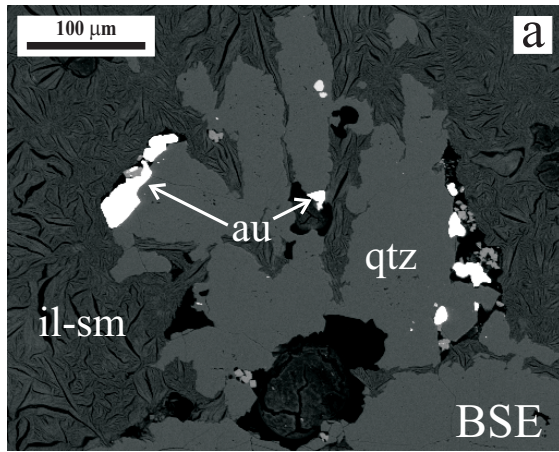
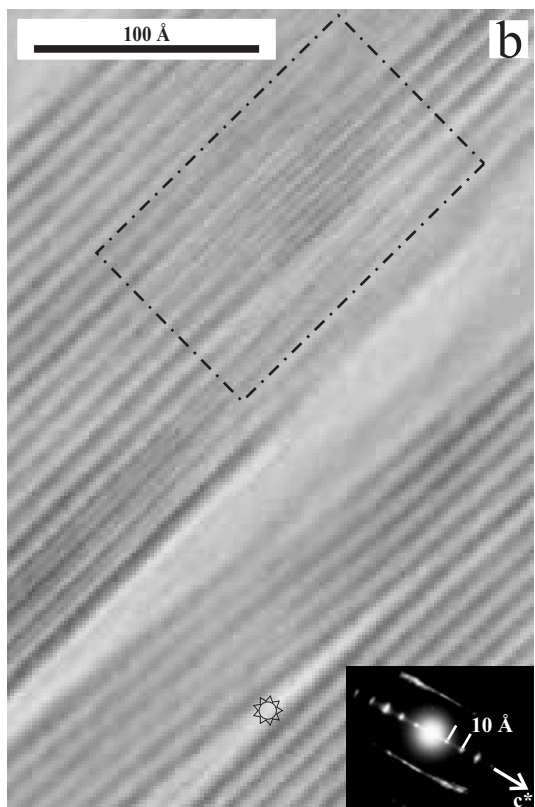
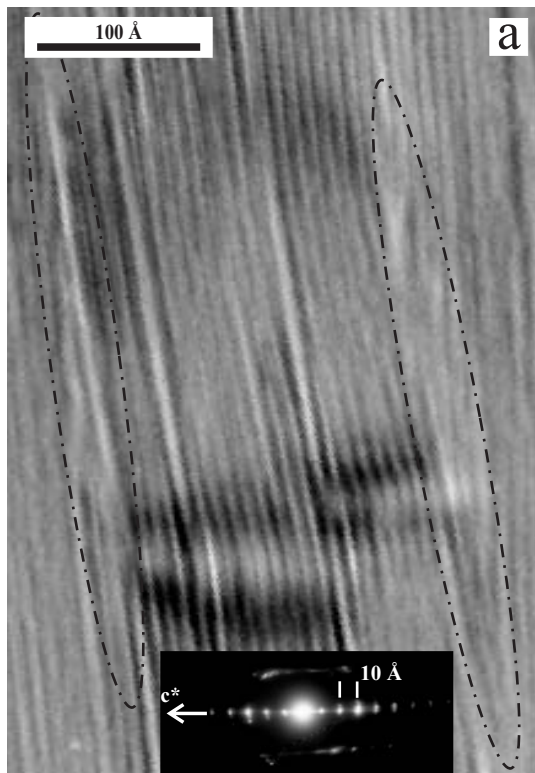
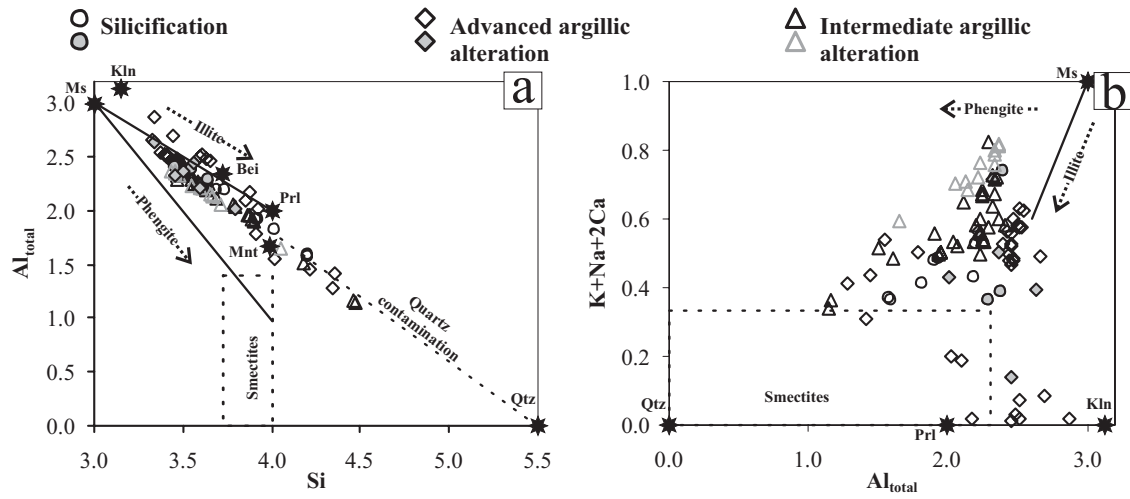


Figure 10. Carrillo et al



# Figure 11. Carrillo et al



# Figure 12. Carrillo et al

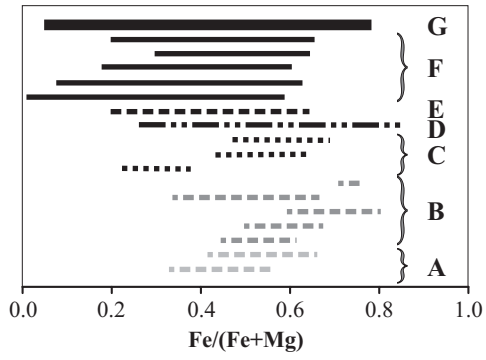


# Figure 13. Carrillo et al

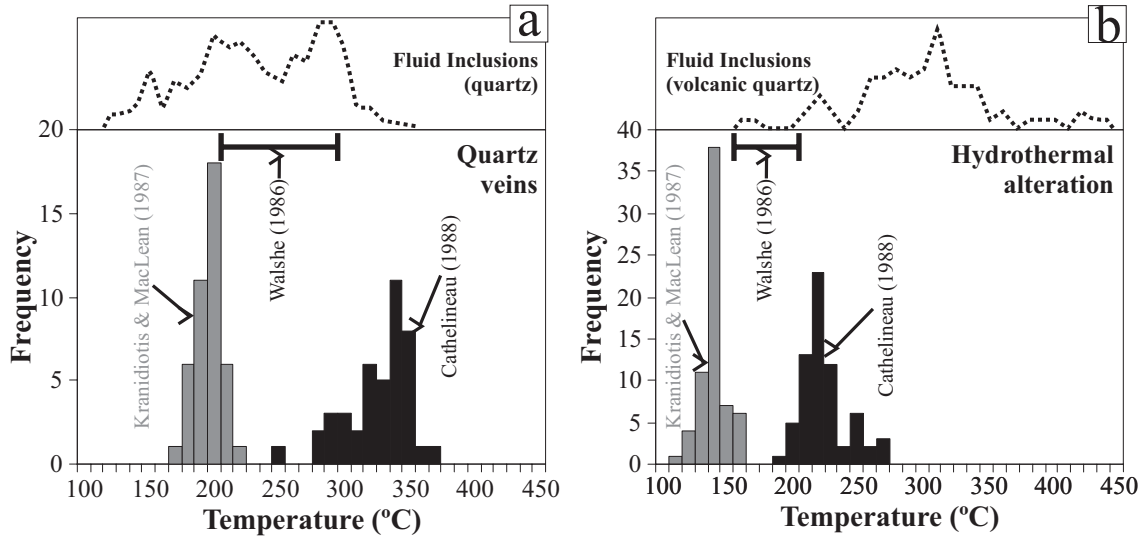


Table 1.

|                                 | Veins | Sericitic alteration                                | Chloritic alteration                           | Silicification | Advanced argillic alteration | Intermediate argillic alteration |
|---------------------------------|-------|---|--|----------------|------------------------------|----------------------------------|
| Chlorite                        | XX    | X<br>(maphic phenocrysts)                           | XXX<br>(matrix and <u>maphic phenocrysts</u> ) |                |                              |                                  |
| Mica                            | XX    | XXX<br>(matrix, plagioclase and maphic phenocrysts) | X<br>(matrix and <u>plagioclase</u> )          |                | XX                           | XX                               |
| Interstratified illite-smectite |       |   |  | X              | X                            | X                                |
| Kaolinite                       |       |   |  |                | XX                           |                                  |
| Pyrophyllite                    |       |   |  |                | XX                           |                                  |

X: scarce; XX: abundant; XXX: very abundant

Table 2.

| % weight                       | Veins (n=43) |             |             |             | Alteration (n=67) |             |             |             | Transitional (n=36) |             |             |             | Propylitic (n=41) |             |             |             |
|--------------------------------|--------------|-------------|-------------|-------------|-------------------|-------------|-------------|-------------|---------------------|-------------|-------------|-------------|-------------------|-------------|-------------|-------------|
|                                | Min          | Max         | Ave         | S.D.        | Min               | Max         | Ave         | S.D.        | Min                 | Max         | Ave         | S.D.        | Min               | Max         | Ave         | S.D.        |
| SiO <sub>2</sub>               | 20.05        | 26.84       | 24.60       | 1.20        | 26.73             | 33.48       | 30.35       | 1.19        | 23.94               | 28.87       | 27.22       | 1.23        | 29.18             | 34.99       | 31.45       | 1.50        |
| TiO <sub>2</sub>               | 0.01         | 0.06        | 0.03        | 0.01        | 0.00              | 0.54        | 0.03        | 0.07        | 0.00                | 0.07        | 0.02        | 0.01        | 0.00              | 23.00       | 4.34        | 8.20        |
| Al <sub>2</sub> O <sub>3</sub> | 13.91        | 21.65       | 19.53       | 1.73        | 16.41             | 20.55       | 18.43       | 1.02        | 16.20               | 20.94       | 19.30       | 1.17        | 0.00              | 21.13       | 13.98       | 7.52        |
| FeO                            | 24.67        | 35.83       | 30.94       | 2.82        | 2.68              | 21.73       | 14.71       | 4.39        | 18.97               | 27.30       | 22.50       | 2.40        | 12.38             | 22.17       | 17.53       | 2.46        |
| MgO                            | 5.71         | 11.68       | 8.81        | 1.84        | 18.32             | 30.77       | 22.36       | 2.85        | 11.38               | 18.09       | 15.09       | 1.90        | 13.82             | 20.53       | 18.12       | 1.31        |
| MnO                            | 0.22         | 1.05        | 0.50        | 0.23        | 0.12              | 0.80        | 0.35        | 0.15        | 0.39                | 0.77        | 0.55        | 0.10        | 0.07              | 0.72        | 0.46        | 0.16        |
| CaO                            | 0.00         | 0.12        | 0.05        | 0.03        | 0.03              | 0.15        | 0.08        | 0.03        | 0.03                | 0.14        | 0.07        | 0.03        | 0.03              | 0.63        | 0.23        | 0.16        |
| K <sub>2</sub> O               | 0.00         | 0.26        | 0.05        | 0.05        | 0.00              | 0.47        | 0.07        | 0.09        | 0.01                | 0.16        | 0.07        | 0.04        | 0.03              | 2.34        | 0.48        | 0.46        |
| Na <sub>2</sub> O              | 0.00         | 0.09        | 0.04        | 0.03        | 0.00              | 0.09        | 0.03        | 0.02        | 0.00                | 0.08        | 0.03        | 0.02        | 0.01              | 0.39        | 0.08        | 0.07        |
| a.p.u.f.                       |              |             |             |             |                   |             |             |             |                     |             |             |             |                   |             |             |             |
| Si                             | 2.65         | 3.05        | 2.79        | 0.08        | 2.89              | 3.14        | 3.05        | 0.05        | 2.86                | 2.99        | 2.92        | 0.04        | 3.01              | 3.61        | 3.19        | 0.13        |
| Ti                             | 0.00         | 0.01        | 0.00        | 0.00        | 0.00              | 0.04        | 0.00        | 0.01        | 0.00                | 0.01        | 0.00        | 0.00        | 0.00              | 0.00        | 0.00        | 0.00        |
| <sup>IV</sup> Al               | 0.95         | 1.35        | 1.21        | 0.08        | 0.86              | 1.11        | 0.95        | 0.05        | 1.01                | 1.14        | 1.08        | 0.04        | 0.39              | 0.99        | 0.81        | 0.13        |
| <sup>VI</sup> Al               | 1.15         | 1.52        | 1.40        | 0.07        | 1.09              | 1.41        | 1.23        | 0.08        | 1.23                | 1.50        | 1.36        | 0.07        | 1.06              | 2.03        | 1.38        | 0.19        |
| Fe                             | 2.41         | 3.40        | 2.94        | 0.27        | 0.21              | 1.86        | 1.24        | 0.38        | 1.70                | 2.43        | 2.02        | 0.23        | 1.02              | 1.92        | 1.49        | 0.22        |
| Mg                             | 0.98         | 1.91        | 1.49        | 0.28        | 2.79              | 4.26        | 3.34        | 0.34        | 2.10                | 2.80        | 2.41        | 0.22        | 2.03              | 3.07        | 2.74        | 0.20        |
| Mn                             | 0.02         | 0.10        | 0.05        | 0.02        | 0.01              | 0.07        | 0.03        | 0.01        | 0.04                | 0.07        | 0.05        | 0.01        | 0.01              | 0.06        | 0.04        | 0.01        |
| Vacancies                      | 0.04         | 0.25        | 0.12        | 0.04        | 0.07              | 0.29        | 0.16        | 0.05        | 0.09                | 0.24        | 0.16        | 0.04        | 0.09              | 0.87        | 0.35        | 0.17        |
| Ca                             | 0.00         | 0.01        | 0.01        | 0.00        | 0.00              | 0.01        | 0.01        | 0.00        | 0.00                | 0.02        | 0.01        | 0.00        | 0.00              | 0.07        | 0.03        | 0.02        |
| K                              | 0.00         | 0.04        | 0.01        | 0.01        | 0.00              | 0.06        | 0.01        | 0.01        | 0.00                | 0.02        | 0.01        | 0.01        | 0.00              | 0.29        | 0.06        | 0.06        |
| Na                             | 0.00         | 0.02        | 0.01        | 0.01        | 0.00              | 0.02        | 0.01        | 0.00        | 0.00                | 0.02        | 0.01        | 0.00        | 0.00              | 0.08        | 0.02        | 0.01        |
| <b>K+Na+2Ca</b>                | <b>0.00</b>  | <b>0.07</b> | <b>0.03</b> | <b>0.02</b> | <b>0.01</b>       | <b>0.09</b> | <b>0.03</b> | <b>0.01</b> | <b>0.01</b>         | <b>0.05</b> | <b>0.03</b> | <b>0.01</b> | <b>0.01</b>       | <b>0.31</b> | <b>0.10</b> | <b>0.07</b> |

n: number of analysis; Min: minimum.; Max: maximum.; Ave: average; S.D.: (standard deviation). Veins: chlorite from the quartz veins with sulphides; Alteration: Chlorite from the hydrothermal alteration related to quartz veins with sulphides; Transitional: chlorite from the quartz veins but originated in the hydrothermal alteration ("xenocrysts"). Propylitic: chlorite from the most marginal zones of the Palai-Islica deposit, in areas of propylitic/regional low temperature alteration.

Table 3.

| % weight                       | Veins-neo. (n=28) |       |       |      | Veins-tran (n=33) |       |       |      | Alteration - c.P. (n=32) |       |       |      | Alteration - f.P. (n=6) |       |       |      | Alteration - Map. (n=12) |       |       |      |
|--------------------------------|-------------------|-------|-------|------|-------------------|-------|-------|------|--------------------------|-------|-------|------|-------------------------|-------|-------|------|--------------------------|-------|-------|------|
|                                | Min               | Max   | Ave   | S.D. | Min               | Max   | Ave   | S.D. | Min                      | Max   | Ave   | S.D. | Min                     | Max   | Ave   | S.D. | Min                      | Max   | Ave   | S.D. |
| SiO <sub>2</sub>               | 49.12             | 53.75 | 50.92 | 1.02 | 47.99             | 52.57 | 50.57 | 1.11 | 49.78                    | 52.98 | 51.22 | 0.84 | 50.32                   | 52.66 | 51.35 | 0.85 | 50.10                    | 52.55 | 51.80 | 0.74 |
| Al <sub>2</sub> O <sub>3</sub> | 26.93             | 35.37 | 32.93 | 1.89 | 29.99             | 35.37 | 32.83 | 1.44 | 31.70                    | 35.16 | 33.42 | 0.93 | 29.86                   | 31.62 | 30.67 | 0.60 | 30.26                    | 33.81 | 32.93 | 1.08 |
| TiO <sub>2</sub>               | 0.04              | 0.22  | 0.08  | 0.04 | 0.02              | 0.09  | 0.06  | 0.02 | 0.00                     | 0.07  | 0.03  | 0.02 | 0.04                    | 0.07  | 0.05  | 0.01 | 0.02                     | 0.05  | 0.03  | 0.01 |
| FeO                            | 0.30              | 5.89  | 1.15  | 1.32 | 0.28              | 2.37  | 0.78  | 0.48 | 0.18                     | 2.58  | 0.76  | 0.67 | 0.45                    | 0.74  | 0.57  | 0.10 | 0.84                     | 1.35  | 0.97  | 0.14 |
| MgO                            | 0.74              | 2.57  | 1.14  | 0.47 | 0.71              | 3.81  | 1.58  | 0.86 | 0.62                     | 2.21  | 1.18  | 0.40 | 2.28                    | 3.52  | 2.83  | 0.52 | 0.94                     | 1.71  | 1.16  | 0.25 |
| MnO                            | 0.00              | 0.05  | 0.01  | 0.01 | 0.00              | 0.07  | 0.02  | 0.02 | 0.00                     | 0.08  | 0.03  | 0.02 | 0.04                    | 0.08  | 0.06  | 0.02 | 0.00                     | 0.02  | 0.00  | 0.01 |
| CaO                            | 0.02              | 0.45  | 0.11  | 0.10 | 0.04              | 0.26  | 0.12  | 0.05 | 0.05                     | 0.51  | 0.13  | 0.12 | 0.33                    | 0.40  | 0.35  | 0.03 | 0.06                     | 0.26  | 0.20  | 0.06 |
| K <sub>2</sub> O               | 7.94              | 9.95  | 9.10  | 0.44 | 7.41              | 9.73  | 8.81  | 0.68 | 7.35                     | 9.17  | 8.47  | 0.63 | 8.34                    | 8.86  | 8.62  | 0.20 | 7.30                     | 8.77  | 8.05  | 0.43 |
| Na <sub>2</sub> O              | 0.04              | 0.30  | 0.16  | 0.07 | 0.08              | 0.78  | 0.23  | 0.16 | 0.07                     | 1.11  | 0.34  | 0.30 | 0.12                    | 0.18  | 0.15  | 0.03 | 0.08                     | 0.82  | 0.21  | 0.19 |
| F                              | 0.00              | 0.33  | 0.18  | 0.08 | 0.10              | 0.37  | 0.21  | 0.05 | 0.00                     | 0.28  | 0.06  | 0.08 | 0.03                    | 0.15  | 0.10  | 0.04 | 0.00                     | 0.14  | 0.05  | 0.05 |
| Cl                             | 0.00              | 0.09  | 0.01  | 0.02 | 0.00              | 0.05  | 0.02  | 0.01 | 0.00                     | 0.05  | 0.02  | 0.01 | 0.00                    | 0.00  | 0.00  | 0.00 | 0.00                     | 0.06  | 0.02  | 0.01 |
| Total                          | 92.14             | 98.97 | 95.80 | 1.67 | 92.14             | 97.62 | 95.23 | 1.49 | 92.07                    | 97.62 | 95.66 | 1.22 | 92.99                   | 96.52 | 94.73 | 1.53 | 91.86                    | 96.59 | 95.41 | 1.37 |
| O=F                            | 0.00              | 0.14  | 0.08  | 0.03 | 0.04              | 0.15  | 0.09  | 0.02 | 0.00                     | 0.12  | 0.03  | 0.03 | 0.01                    | 0.06  | 0.04  | 0.02 | 0.00                     | 0.06  | 0.02  | 0.02 |
| O=Cl                           | 0.00              | 0.02  | 0.00  | 0.00 | 0.00              | 0.01  | 0.00  | 0.00 | 0.00                     | 0.01  | 0.00  | 0.00 | 0.00                    | 0.00  | 0.00  | 0.00 | 0.00                     | 0.01  | 0.00  | 0.00 |
| a.p.u.f.                       |                   |       |       |      |                   |       |       |      |                          |       |       |      |                         |       |       |      |                          |       |       |      |
| Si                             | 3.26              | 3.44  | 3.32  | 0.05 | 3.23              | 3.37  | 3.31  | 0.03 | 3.24                     | 3.39  | 3.32  | 0.03 | 3.36                    | 3.39  | 3.37  | 0.01 | 3.31                     | 3.40  | 3.35  | 0.02 |
| <sup>IV</sup> Al               | 0.56              | 0.74  | 0.69  | 0.05 | 0.63              | 0.77  | 0.69  | 0.03 | 0.61                     | 0.76  | 0.68  | 0.02 | 0.61                    | 0.64  | 0.63  | 0.01 | 0.60                     | 0.69  | 0.65  | 0.02 |
| <sup>VI</sup> Al               | 1.75              | 1.93  | 1.87  | 0.05 | 1.71              | 1.95  | 1.85  | 0.06 | 1.79                     | 1.94  | 1.86  | 0.03 | 1.71                    | 1.87  | 1.74  | 0.03 | 1.77                     | 1.90  | 1.87  | 0.04 |
| Ti                             | 0.00              | 0.01  | 0.00  | 0.00 | 0.00              | 0.00  | 0.00  | 0.00 | 0.00                     | 0.00  | 0.00  | 0.00 | 0.00                    | 0.00  | 0.00  | 0.00 | 0.00                     | 0.00  | 0.00  | 0.00 |
| Fe                             | 0.02              | 0.34  | 0.06  | 0.08 | 0.01              | 0.13  | 0.04  | 0.03 | 0.01                     | 0.14  | 0.04  | 0.04 | 0.02                    | 0.04  | 0.03  | 0.01 | 0.04                     | 0.07  | 0.05  | 0.01 |
| Mg                             | 0.07              | 0.25  | 0.11  | 0.04 | 0.07              | 0.36  | 0.15  | 0.08 | 0.06                     | 0.22  | 0.11  | 0.04 | 0.22                    | 0.34  | 0.28  | 0.05 | 0.09                     | 0.17  | 0.11  | 0.03 |
| Mn                             | 0.00              | 0.00  | 0.00  | 0.00 | 0.00              | 0.00  | 0.00  | 0.00 | 0.00                     | 0.00  | 0.00  | 0.00 | 0.00                    | 0.00  | 0.00  | 0.00 | 0.00                     | 0.00  | 0.00  | 0.00 |
| <sup>VI</sup> Σ                | 1.97              | 2.02  | 2.00  | 0.01 | 2.01              | 2.15  | 2.05  | 0.04 | 1.99                     | 2.10  | 2.03  | 0.02 | 2.02                    | 2.10  | 2.06  | 0.03 | 2.01                     | 2.07  | 2.03  | 0.01 |
| Ca                             | 0.00              | 0.03  | 0.01  | 0.01 | 0.00              | 0.02  | 0.01  | 0.00 | 0.00                     | 0.03  | 0.01  | 0.01 | 0.02                    | 0.03  | 0.02  | 0.00 | 0.00                     | 0.02  | 0.01  | 0.00 |
| K                              | 0.68              | 0.82  | 0.76  | 0.03 | 0.60              | 0.82  | 0.74  | 0.06 | 0.60                     | 0.77  | 0.70  | 0.05 | 0.69                    | 0.74  | 0.72  | 0.02 | 0.62                     | 0.74  | 0.67  | 0.04 |
| Na                             | 0.01              | 0.04  | 0.02  | 0.01 | 0.01              | 0.10  | 0.03  | 0.02 | 0.01                     | 0.15  | 0.04  | 0.04 | 0.02                    | 0.02  | 0.02  | 0.00 | 0.01                     | 0.11  | 0.03  | 0.02 |
| K+Na+2Ca                       | 0.75              | 0.85  | 0.79  | 0.03 | 0.69              | 0.86  | 0.78  | 0.05 | 0.65                     | 0.84  | 0.76  | 0.05 | 0.75                    | 0.81  | 0.79  | 0.02 | 0.68                     | 0.86  | 0.72  | 0.05 |
| F                              | 0.00              | 0.07  | 0.04  | 0.02 | 0.02              | 0.08  | 0.04  | 0.01 | 0.00                     | 0.06  | 0.01  | 0.02 | 0.01                    | 0.03  | 0.02  | 0.01 | 0.00                     | 0.03  | 0.01  | 0.01 |
| Cl                             | 0.00              | 0.01  | 0.00  | 0.00 | 0.00              | 0.01  | 0.00  | 0.00 | 0.00                     | 0.01  | 0.00  | 0.00 | 0.00                    | 0.00  | 0.00  | 0.00 | 0.00                     | 0.01  | 0.00  | 0.00 |

n: number of analysis; Min: minimum.; Max: maximum.; Ave: average; S.D.: (standard deviation). Veins-neo: mica from the quartz veins apparently neoformed; Veins-tran: mica from the quartz veins formed primary in hydrothermal alteration; Alteration-c.P.: relatively "coarse" mica replacing plagioclase from the hydrothermal alteration related to quartz veins; Alteration-f.P.: "fine" mica replacing plagioclase from the hydrothermal alteration related to quartz veins; Alteration-Map.: mica replacing maphic phenocrysts from the hydrothermal alteration related to quartz veins.

Table 4.

| % weight                       | Silicification (n=8) |       |       |      | Advanced argillic (n=31) |       |       |      | Intermediate argillic (n=31) |       |       |      |
|--------------------------------|----------------------|-------|-------|------|--------------------------|-------|-------|------|------------------------------|-------|-------|------|
|                                | Min                  | Max   | Ave   | S.D. | Min                      | Max   | Ave   | S.D. | Min                          | Max   | Ave   | S.D. |
| SiO <sub>2</sub>               | 49.45                | 64.40 | 59.12 | 5.24 | 41.64                    | 62.63 | 50.97 | 4.68 | 47.36                        | 66.55 | 53.61 | 4.55 |
| Al <sub>2</sub> O <sub>3</sub> | 19.27                | 28.37 | 24.68 | 3.00 | 14.30                    | 35.29 | 27.84 | 6.05 | 10.30                        | 30.78 | 25.91 | 4.85 |
| TiO <sub>2</sub>               | 0.00                 | 0.02  | 0.01  | 0.01 | 0.00                     | 0.20  | 0.03  | 0.06 | 0.01                         | 0.38  | 0.06  | 0.06 |
| FeO                            | 0.11                 | 0.19  | 0.15  | 0.02 | 0.02                     | 4.16  | 0.56  | 0.81 | 0.17                         | 0.97  | 0.44  | 0.18 |
| MgO                            | 0.31                 | 0.51  | 0.41  | 0.06 | 0.04                     | 1.57  | 0.81  | 0.48 | 0.33                         | 1.84  | 1.11  | 0.49 |
| MnO                            | 0.00                 | 0.02  | 0.01  | 0.01 | 0.00                     | 0.03  | 0.01  | 0.01 | 0.00                         | 0.07  | 0.02  | 0.02 |
| CaO                            | 0.24                 | 0.48  | 0.33  | 0.08 | 0.03                     | 0.82  | 0.24  | 0.21 | 0.03                         | 0.85  | 0.26  | 0.21 |
| K <sub>2</sub> O               | 3.39                 | 5.29  | 4.41  | 0.66 | 0.05                     | 7.19  | 3.78  | 2.43 | 2.67                         | 9.05  | 6.13  | 1.43 |
| Na <sub>2</sub> O              | 0.16                 | 0.30  | 0.22  | 0.05 | 0.03                     | 0.81  | 0.16  | 0.15 | 0.05                         | 0.23  | 0.15  | 0.05 |
| Cl                             | 0.01                 | 0.08  | 0.05  | 0.02 | 0.00                     | 0.21  | 0.06  | 0.05 | 0.02                         | 0.26  | 0.10  | 0.07 |
| F                              | 0.01                 | 0.12  | 0.06  | 0.04 | 0.00                     | 0.20  | 0.08  | 0.06 | 0.04                         | 0.28  | 0.14  | 0.07 |
| total                          | 81.55                | 97.12 | 89.44 | 5.21 | 69.01                    | 98.04 | 84.54 | 9.24 | 62.36                        | 96.37 | 87.95 | 7.90 |
| O=F                            | 0.01                 | 0.05  | 0.02  | 0.02 | 0.00                     | 0.09  | 0.03  | 0.03 | 0.02                         | 0.12  | 0.06  | 0.03 |
| O=Cl                           | 0.00                 | 0.02  | 0.01  | 0.00 | 0.00                     | 0.05  | 0.01  | 0.01 | 0.00                         | 0.06  | 0.02  | 0.02 |
| a.p.u.f.                       |                      |       |       |      |                          |       |       |      |                              |       |       |      |
| Si                             | 3.65                 | 4.21  | 3.92  | 0.20 | 3.32                     | 4.36  | 3.62  | 0.29 | 3.47                         | 4.47  | 3.72  | 0.27 |
| <sup>IV</sup> Al               | 0.00                 | 0.35  | 0.08  | 0.20 | 0.00                     | 0.68  | 0.38  | 0.29 | 0.00                         | 0.53  | 0.28  | 0.27 |
| <sup>VI</sup> Al               | 1.78                 | 1.92  | 1.85  | 0.05 | 1.57                     | 2.21  | 1.93  | 0.15 | 1.61                         | 1.92  | 1.81  | 0.07 |
| Ti                             | 0.00                 | 0.00  | 0.00  | 0.00 | 0.00                     | 0.01  | 0.00  | 0.00 | 0.00                         | 0.02  | 0.00  | 0.00 |
| Fe                             | 0.01                 | 0.01  | 0.01  | 0.00 | 0.00                     | 0.27  | 0.03  | 0.05 | 0.01                         | 0.06  | 0.03  | 0.01 |
| Mg                             | 0.03                 | 0.05  | 0.04  | 0.01 | 0.01                     | 0.15  | 0.08  | 0.05 | 0.03                         | 0.20  | 0.12  | 0.05 |
| Mn                             | 0.00                 | 0.00  | 0.00  | 0.00 | 0.00                     | 0.00  | 0.00  | 0.00 | 0.00                         | 0.00  | 0.00  | 0.00 |
| <sup>VI</sup> Σ                | 1.61                 | 1.97  | 1.85  | 0.13 | 1.80                     | 2.23  | 2.04  | 0.09 | 1.80                         | 2.06  | 1.96  | 0.07 |
| Ca                             | 0.02                 | 0.03  | 0.02  | 0.01 | 0.00                     | 0.06  | 0.02  | 0.02 | 0.00                         | 0.06  | 0.02  | 0.02 |
| K                              | 0.30                 | 0.45  | 0.37  | 0.06 | 0.00                     | 0.57  | 0.33  | 0.20 | 0.32                         | 0.79  | 0.54  | 0.11 |
| Na                             | 0.02                 | 0.04  | 0.03  | 0.00 | 0.00                     | 0.13  | 0.02  | 0.02 | 0.01                         | 0.03  | 0.02  | 0.01 |
| Interlámina                    | 0.37                 | 0.53  | 0.45  | 0.06 | 0.01                     | 0.63  | 0.39  | 0.21 | 0.34                         | 0.83  | 0.58  | 0.10 |
| F                              | 0.00                 | 0.03  | 0.01  | 0.01 | 0.00                     | 0.05  | 0.02  | 0.02 | 0.01                         | 0.06  | 0.03  | 0.01 |
| Cl                             | 0.00                 | 0.01  | 0.01  | 0.00 | 0.00                     | 0.03  | 0.01  | 0.01 | 0.00                         | 0.03  | 0.01  | 0.01 |

n: number of analysis; Min: minimum.; Max: maximum.; Ave: average; S.D.: (standard deviation). Silicification: illite/interstratified illite-smectite from the silicification; Advanced argillic: Phyllosilicates from the advanced argillic alteration; Intermediate argillic: Phyllosilicates from the intermediate argillic alteration.

Table 5.

|                  | S.   | S.   | S.   | A.A.A. | A.A.A. | A.A.A. | A.A.A. | A.A.A. | A.A.A. |
|------------------|------|------|------|--------|--------|--------|--------|--------|--------|
| Si               | 3.45 | 3.55 | 3.64 | 3.33   | 3.56   | 3.46   | 3.80   | 3.50   | 3.60   |
| <sup>IV</sup> Al | 0.55 | 0.45 | 0.36 | 2.63   | 2.45   | 2.32   | 2.01   | 2.37   | 2.22   |
| <sup>VI</sup> Al | 1.85 | 1.93 | 1.93 | 0.00   | 0.00   | 0.00   | 0.00   | 0.00   | 0.00   |
| Fe               | 0.01 | 0.01 | 0.01 | 0.00   | 0.00   | 0.01   | 0.03   | 0.00   | 0.00   |
| Mg               | 0.12 | 0.13 | 0.10 | 0.19   | 0.14   | 0.24   | 0.14   | 0.19   | 0.19   |
| <sup>VI</sup> Σ  | 1.98 | 2.07 | 2.04 | 2.15   | 2.15   | 2.02   | 1.98   | 2.06   | 2.01   |
| Ca               |      |      |      | 0.00   | 0.00   | 0.00   | 0.00   | 0.00   | 0.09   |
| K                | 0.55 | 0.39 | 0.25 | 0.39   | 0.14   | 0.60   | 0.38   | 0.50   | 0.39   |
| Na               | 0.19 | 0.00 | 0.11 | 0.00   | 0.00   | 0.11   | 0.05   | 0.00   | 0.00   |
| K+Na+2Ca         | 0.74 | 0.39 | 0.36 | 0.39   | 0.14   | 0.72   | 0.43   | 0.50   | 0.57   |

S.: Illite/ interstratified illite-smectite from the silicification analyzed in an ion milled sample preparation; A.A.A.: mica/mica-smectite interstratified from the advanced argillic alteration analyzed in a formvar Cu grid.

1001 **FIGURE CAPTIONS**

1002 **Figure 1:**

1003 (a) Cabo de Gata – Cartagena volcanic province in SE of Spain with the location of  
1004 the most important ore deposits volcanic belt (adapted from Lopez-Ruiz and  
1005 Rodriguez-Badiola, 1980): (1) Cabo de Gata. (2) Rodalquilar. (3) Carboneras (Palai-  
1006 Islica). (4) Herrerías and Sierra Almagrera. (5) Aguilas. (6) Mazarrón. (7) Cartagena.  
1007 (b) Schematic geological map showing the location of the Palai-Islica deposit and  
1008 main geological units (adapted from IGME, 1974).

1009

1010 **Figure 2:**

1011 Schematic picture of Palai-Islica deposit which include the position of the different  
1012 kinds of mineralisations which appear on it. In the silicification, an arrow indicates a  
1013 phyllosilicate micro-vein.

1014

1015 **Figure 3:**

1016 Transmitted light (parallel and crossed polarized) and backscattered electron (BSE)  
1017 photomicrograph of chlorites. (a and b) Spherulitic aggregates of chlorite (chl)  
1018 intergrowing with coarse quartz and sulphides in the veins. In the BSE image (b) it  
1019 is observed dark cores and bright rims in chlorite and mica (mi) interstitial and maybe  
1020 replacing chlorite. (c and d) Prismatic and basal section of hornblende (in “maximum  
1021 of illumination” and “extinction” positions) replaced by coherent orientated chlorite  
1022 in the hydrothermal alteration related to quartz veins. (e) Chlorite precedent of  
1023 hornblende replacement inside a quartz vein. (f) Incipient replacing of hornblende  
1024 (hbl) by chlorite (chl) in the propylitic alteration.

1025

1026 **Figure 4:**

1027 Binary diagrams showing compositional variations, expressed at atoms per unit  
1028 formula, between tetrahedral and octahedral cations and interlayer cations and  
1029 vacancies in the different types of chlorites. It is showed for comparison the  
1030 Fe/(Fe+Mg) ratio of the unaltered volcanic rock and phenocrysts (data from  
1031 Fernández Soler, 1996) which hosts the Palai-Islica deposit. EPMA analyses are  
1032 plotted in black without fill, TEM-AEM analyses in dark grey fill, and SEM analyses  
1033 in grey color without fill. The influence of mica contamination and correlation line in  
1034 chlorite analyses is shown by a dotted and solid line respectively if (e).

1035

1036 **Figure 5:**

1037 Transmitted light (plane-polarized and cross-polarized light) and TEM  
1038 photomicrographs of mica. (a) Micro-veins of mica of sub-microscopic character  
1039 inside a quartz vein. (b) Coarse mica intergrowing with quartz. Sub-microscopic (c)  
1040 and micron size (d) mica replacing a volcanic plagioclase inside hydrothermal  
1041 alteration related to quartz veins. In (d) it is observed orientated crystals parallel  
1042 to cleavage plagioclase planes, which in low magnification TEM image (e) shown a

1043 prismatic morphology. Hornblende replaced by fine grained disorientated mica (f)  
1044 and coherent orientated mica (g) in the hydrothermal alteration related to quartz  
1045 veins. (h) Maphic phenocrysts prismatic section replaced by orientated chlorite and  
1046 mica. (i) TEM lattice-fringe image of chlorite (14 Å) with coherent mica layers (10  
1047 Å, marked with an arrow) in a zone of mica-chlorite intergrowth similar to (h). (j)  
1048 Zone of transition between a quartz vein and the related hydrothermal alteration. It is  
1049 observed coarse grained mica provably originated by a transformation of a maphic  
1050 phenocrysts and fined mica precedent from plagioclase transformation (inside a  
1051 square in the left down corner).

1052

1053 **Figure 6:**

1054 (a) XRD patterns of <2µm bulk sample fraction from hydrothermal alteration (down)  
1055 and of mica replacing plagioclase separated by microdrilling (up) with vertical lines  
1056 showing reflections of different polytypes according to Bailey (1980) and Moore and  
1057 Reynolds (1997). 2.58 Å and 2.80Å peaks are marked since  $I_{2.80}/I_{2.58}$  has been related  
1058 to  $2M/(2M+1Md)$  (Maxwell and Hower, 1967). 2.42 Å, 2.45 Å (ordered) and 2.38 Å  
1059 (disordef) peaks are marked in order to estimate disorder of the n60° kind (Moore  
1060 and Reynolds (1997).

1061 (b) SAED patterns of mica showing 2M polytype (left) and 3T polytype (right) from  
1062 mica replacing plagioclase in the hydrothermal alteration and disseminated mica in a  
1063 vein, respectively.

1064

1065 **Figure 7:**

1066 Binary diagrams showing compositional variations, expressed at atoms per unit  
1067 formula, between major elements in the different types of mica in the quartz veins  
1068 and related hydrothermal alteration. It is showed for comparison the muscovite  
1069 composition (Ms) and different chemical vectors: illite substitution ( $Si_{1-x}Al^{IV}_xK_{-x}$ ),  
1070 phengite substitution ( $(Fe+Mg)_1Si_1^{VI}Al_1^{IV}Al_1$ ), ferrimuscovite substitution  
1071 ( $Fe^{3+}_{-1}Al_1^{IV}$ ). EPMA-WDX analyses are plotted in black without fill, TEM-AEM  
1072 analyses in dark grey fill, and SEM-EDX analyses in grey color without fill.

1073

1074 **Figure 8:**

1075 Frequency histograms for (a) K and (d) F content expressed at atoms per formula  
1076 unit in the different types of analyzed mica. EPMA-WDX analyses are plotted in  
1077 black columns, TEM-AEM analyses in dark grey color columns, and SEM-EDX  
1078 analyses are in light grey color columns.

1079

1080 **Figure 9:**

1081 Backscattered electron (BSE) images of illite/illite-smectite (il-sm) in the  
1082 silicification. In (a), illite-smectite appears together native gold grains (au) and  
1083 quartz, while in (b), it is appreciable its chemical zonation.

1084

1085 **Figure 10:**  
1086 HR-TEM (BSE) images of illite/interstratified illite-smectite with 10Å periodicity in  
1087 the silicification and relatively disorder SAED pattern. In (a) it is observed  
1088 termination of several layers in wedge (inside oval). In (b) individual layer  
1089 termination wedge is showed (noted by a start) and also splitting 10Å layers into 5Å  
1090 layers (noted by a dotted square), maybe related with screw dislocation affecting  
1091 interstratified illite-smectite.

1092  
1093 **Figure 11:**  
1094 Binary diagrams showing compositional variations, expressed at atoms per unit  
1095 formula, between Si, Al and K+Na+2Ca of phyllosilicates from the silicification and  
1096 related hydrothermal alteration. It is showed for comparison the muscovite (Ms),  
1097 kaolinite (Kln), pyrophyllite (Prl), beidellite (Bei), montmorillonite (Mnt) and quartz  
1098 (Qtz) composition, and: illite substitution ( $\text{Si}_{1-x}\text{Al}^{\text{IV}}_{x-1}\text{K}_{-1}$ ) and phengite substitution  
1099 ( $(\text{Fe}+\text{Mg})_1\text{Si}_1^{\text{VI}}\text{Al}_1^{\text{IV}}\text{Al}_1$ ) chemical vectors. EPMA-WDX analyses are plotted in  
1100 black, while SEM-EDX analyses are plotted in grey color and TEM-AEM analysis  
1101 in grey filled symbol.

1102  
1103 **Figure 12:**  
1104 Variation of the la relation of Fe/(Fe+Mg) in chlorites from Palai-Islica and from  
1105 different geological settings: (A) metabasites from New Zeland (Copper, 1972);  
1106 metapelites from New Caledonia (Black, 1975); (B) sedimentary rocks and  
1107 metasedimentary rocks from the SE, NW of Spain and Kazahastan (Abad *et al.*,  
1108 2001; 2003a; 2003b); sandstones from Texas (Boles and Franks, 1979), sediments  
1109 from the Gulf Cost (Ahn and Peacor, 1985); (C) Geothermal field in Los Azufres-  
1110 Mexico- (Cathelineau and Nieva, 1985), and Salton Sea-USA- (McDowell and  
1111 Elders, 1980), Pantelleria-Italy- (Fulignati *et al.*, 1997); (D) Hydrothermal vents in  
1112 Atlantic and Pacific mid-ocean ridge (Saccacocia and Gillis, 1995) (E) Altered  
1113 granites (Hecht *et al.*, 1999); (F) Cu veins and stratabound Cu deposits associated to  
1114 basic rocks in the north of Italy –*v.d.*: various deposits- (Zaccarini *et al.*, 2003);  
1115 VHMS deposits from Canada (Kranidiotis and MacLean, 1987), from Iberian Pyrite  
1116 Belt (Sánchez España *et al.*, 2000), and from Morocco (Hibti and Marignac, 2001);  
1117 (G) Palai-Islica Au-Cu epithermal deposit.

1118  
1119 **Figure 13:**  
1120 Frequency histograms of temperature obtained with Kranidiotis and MacLean (1987)  
1121 (grey) and Cathelineau (1988) chlorite geothermometers in (a) quartz veins with  
1122 sulphides and (b) hydrothermal alteration related to quartz veins. A horizontal line  
1123 show the interval of temperatures calculated by Walshe (1986) geothermometer for  
1124 selected analyses which reflect chlorite chemical composition variability. It is also  
1125 showed for comparison Th data of fluid inclusions in quartz from the veins and in  
1126 volcanic quartz phenocrysts in the hydrothermal alteration. The last fluid inclusions

1127 secondary type, but coetaneous with hydrothermal activity. These Th data, not in  
1128 vertical scale, are from Carrillo-Rosúa (2005).  
1129

## TABLE CAPTIONS

1130

**Table 1:**

1131

1132 Summary of distribution of phyllosilicates at the Palai-Islica deposit, in relation to  
1133 the primary mineralogy of the host rock.

1134

**Table 2:**

1135

1136 Chemistry of chlorite analyzed by EPMA in the quartz veins and related  
1137 hydrothermal alteration of the Palai-Islica deposit (normalized to  $O_{10}(OH)_8$ ).

1138

**Table 3:**

1139

1140 Chemistry of mica analyzed by EPMA in the quartz veins and related hydrothermal  
1141 alteration of the Palai-Islica deposit (normalized to  $O_{10}(OH)_2$ ).

1142

**Table 4:**

1143

1144 Chemistry of phyllosilicates analyzed by EPMA in the silicification and related  
1145 hydrothermal alteration of the Palai-Islica deposit (normalized to  $O_{10}(OH)_2$ ).

1146

**Table 5:**

1147

1148 Individual HR-TEM analyses of phyllosilicates from the silicification and advanced  
1149 argillic alteration (normalized to  $O_{10}(OH)_2$ ).

1150